DOI: 10.1002/anie.201300947

Electrochemistry

Bipolar Electrochemistry

*Stephen E. Fosdick, Kyle N. Knust, Karen Scida, and Richard M. Crooks**

Keywords:
electrochemistry · materials science · sensors

In memory of Su-Moon Park

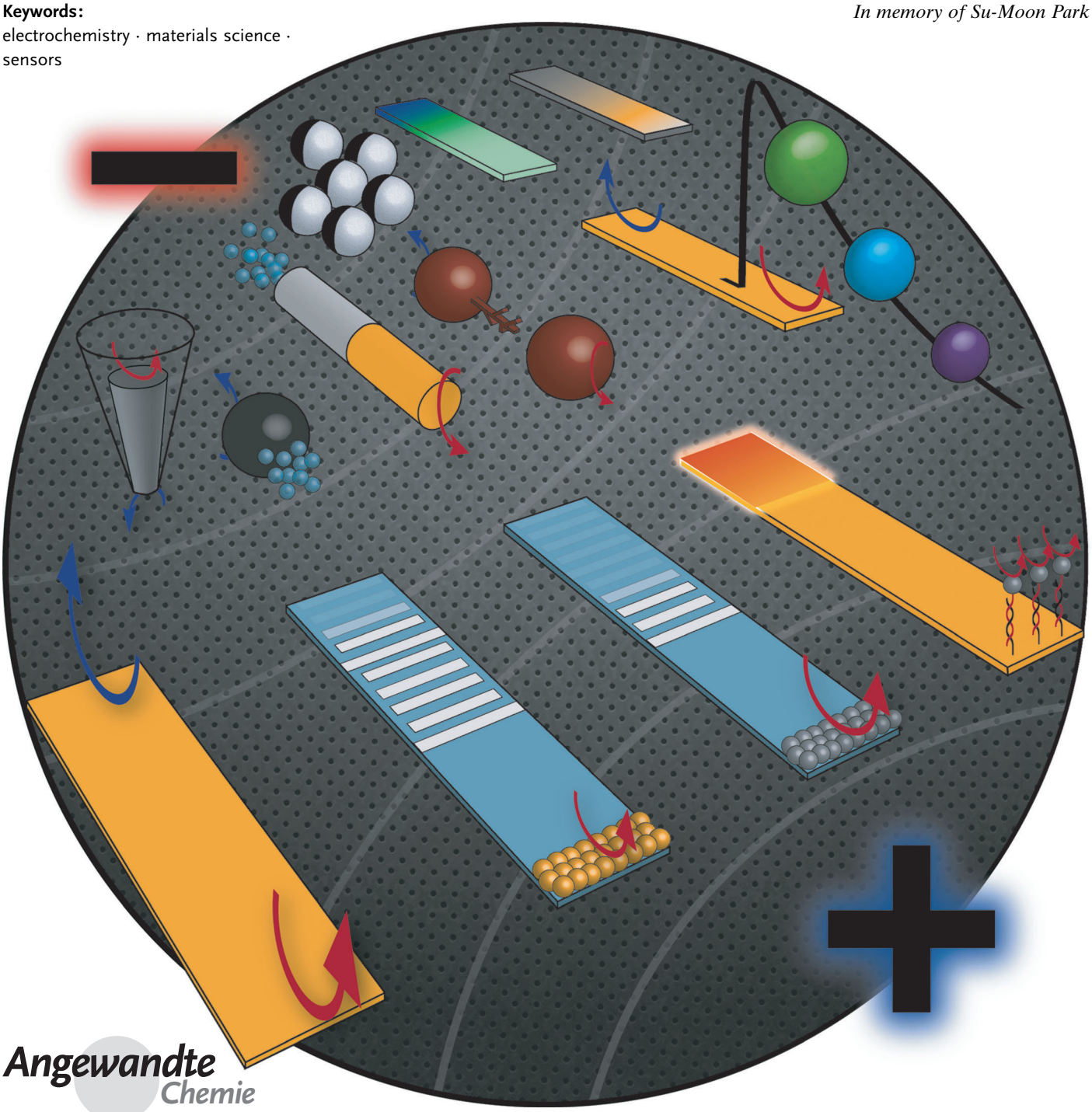

Angewandte International Edition Chemie

A bipolar electrode (BPE) is an electrically conductive material that promotes electrochemical reactions at its extremities (poles) even in the absence of a direct ohmic contact. More specifically, when sufficient voltage is applied to an electrolyte solution in which a BPE is immersed, the potential difference between the BPE and the solution drives oxidation and reduction reactions. Because no direct electrical connection is required to activate redox reactions, large arrays of electrodes can be controlled with just a single DC power supply or even a battery. The wireless aspect of BPEs also makes it possible to electrosynthesize and screen novel materials for a wide variety of applications. Finally, bipolar electrochemistry enables mobile electrodes, dubbed microswimmers, that are able to move freely in solution.

From the Contents

1. Introduction

The objective of this Review is to introduce biological and physical scientists to the concept of bipolar electrochemistry with a view toward expanding its scope in new and interesting directions. This is a worthwhile goal, because the broad adoption of electrochemical methods by those working in other subdisciplines of science in recent years has underscored some shortcomings of existing techniques, apparatuses, and theory. These include the difficulty of making direct electrical contact to nanoscale electrodes, maintaining control over and reading out very large arrays of electrodes simultaneously, controlling electrodes that are mobile in solution, maintaining a non-uniform potential difference over the surface of an electrode, and using electrodes to control local solution potentials. In this Review, we will show that all of these aspects of electrochemistry can be addressed, at least partially, using bipolar electrodes (BPEs).

A more detailed summary of the principles underpinning bipolar electrochemistry will be presented in Section 2, but it is instructive to provide a very brief overview now. Scheme 1 shows a typical experimental configuration used for carrying out bipolar electrochemistry. Here, the driving electrodes apply a uniform electric field across the electrolyte solution, and the resulting faradaic electrochemical reactions at the BPE are shown occurring at the anodic (blue arrow) and cathodic (red arrow) poles of the BPE. As discussed later, the interfacial potential difference between the solution and BPE is highest at the ends of the electrode, so faradaic processes are always observed there first.

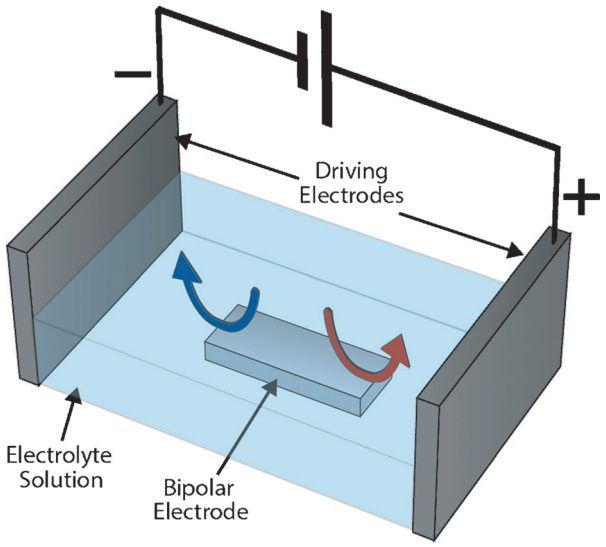

Scheme 1.

Consider the following simple thought experiment based on the electrochemical cell shown in Scheme 1, a platinum BPE, and an aqueous solution containing a dilute, inert electrolyte. When the power supply is turned on to, for example, 1 V, no faradaic reactions are observed at either the driving electrodes or the BPE. However, at a critical voltage that depends on a number of experimental factors, bubbles are observed at the poles of the BPE. Analysis would show that those at the cathodic pole are hydrogen and those at the anodic pole are oxygen. In other words, even though the BPE is an equipotential surface (or nearly so), the electrolysis of water is occurring at its two poles. Importantly, charge must be conserved at the BPE, and therefore the rates of formation of $^1/_2\,O_2$ and H_2 are the same. Faradaic reactions might also occur at the driving electrodes, but although this is usually a nuisance it does not directly affect the BPE. We wish to emphasize that this is an oversimplified version of bipolar electrochemistry, but more details and experimental nuances will be discussed later.

The main focus of the present article is on interesting fundamentals and applications of bipolar electrochemistry

[*] S. E. Fosdick, K. N. Knust, K. Scida, Prof. R. M. Crooks
Department of Chemistry and Biochemistry and the Center for Nano- and Molecular Science and Technology
The University of Texas at Austin
105 E. 24th St., Stop A5300, Austin, TX 78712-1224 (USA)
E-mail: crooks@cm.utexas.edu
Homepage: http://rcrooks.cm.utexas.edu/research/index.html

that have emerged since about the year 2000, but it is important to note that bipolar electrochemistry has been around for many years. Beginning in the 1960s, Fleischmann, Goodridge, Wright, and co-workers described fluidized bed electrodes, where a voltage applied between two driving electrodes enables electrochemical reactions at discrete conductive particles.[1–6] Since these early studies, bipolar fluidized bed electrodes have been used in applications ranging from improving the efficiency of electrosyntheses,[7–9] photoelectrochemical cells,[10,11] and even batteries.[12] Bipolar plate technology is critical for polymeric electrolyte membrane (PEM) fuel cells where the plates form a series of BPEs.[13,14] Additionally, neuronal behavior can also be mimicked using short-circuited microbands which act as a BPE, forming logic gates.[15]

During the past 15 years or so, many interesting bipolar electrochemical experiments have been presented in the literature, and some of these are discussed in a recently published review article.[124] Our own group has explored a number of fundamental aspects and applications of bipolar electrochemistry. For example, Figure 1a is an optical micrograph of a microfabricated BPE array consisting of 1000 electrodes.[16] When a sufficiently large driving voltage is applied to the array, electrogenerated chemiluminescence (ECL) is produced at the anodic pole of each BPE (Figure 1b). The important result of this experiment is that the wireless capabilities of BPEs allow arbitrarily large arrays of electrodes to be powered in a very simple setup.

A number of groups have shown that bipolar electrochemical reactions can be used to induce motion in objects.[17–20] An illustrative example from Kuhn's group is shown in Figure 2.[21–23] Here, bubbles produced by electrochemical reactions (i.e., H_2 or O_2) generate sufficient propulsion to induce the movement of small BPEs. Compositional or chemical gradients can be synthesized on BPEs, as has been elegantly demonstrated by Inagi, Fuchigami, and coworkers, who carried out position-dependent doping of electroactive polymers (Figure 3).[24,25] Our group has also investigated BPEs as a means of enriching and separating charged species electrokinetically. In Figure 4, a single Au BPE is used to locally enrich several different charged markers in a single microchannel.[26] This approach makes it possible to concentrate analytes up to 500000-fold in a highly controlled zone.[27–33] Finally, arrays of BPEs can be used for a variety of sensing and screening applications,[16,34–44] which we will discuss in Section 4. Further explanation and discussion of these types of bipolar electrochemical experiments are included in later sections.

2. Fundamentals of Bipolar Electrochemistry

2.1. Relationship Between Driving Electrodes and a BPE

A key point for understanding wireless bipolar electrochemistry is that the poles of a BPE are oriented in the opposite polarity of the driving electrodes (Scheme 2a). This was clearly demonstrated by Manz and co-workers who placed a Pt wire in a weighing boat filled with a pH indicator solution.[45] As shown in Figure 5a, application of 30 V between the red and blue wires (driving electrodes) causes the pH of the solution at the positive driving electrode (anode, red) to decrease (orange color) due to water oxidation and concomitant production of H^+. Likewise, water reduction at the negative driving electrode (cathode, blue) leads to formation of OH^-, an increase in pH, and the

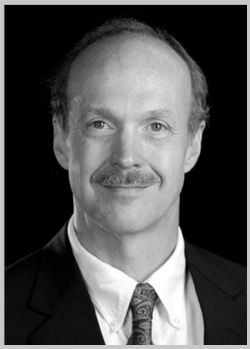

Richard M. Crooks is presently the Robert A. Welch Chair in Materials Chemistry at The University of Texas at Austin. His scientific interests include electrochemistry, chemical sensing, and catalysis. He has published nearly 250 research papers and is the recipient of several awards including the Carl Wagner Memorial Award of the Electrochemical Society and the American Chemical Society Electrochemistry Award.

Kyle N. Knust earned his B.S. in chemistry from the University of Evansville in 2009. He also performed research in the lab of Prof. Dennis G. Peters at Indiana University. He is currently a graduate student in the group of Prof. Richard M. Crooks at The University of Texas at Austin with research focused on bipolar electrochemistry and the development of lab-on-a-chip technologies.

Stephen E. Fosdick received his B.S. in Chemistry from Iowa State University in 2009, where he worked in the lab of Prof. Emily A. Smith. He is currently a graduate student in the group of Prof. Richard M. Crooks, where his current research focuses on the development of electrocatalyst screening platforms using bipolar electrochemistry.

Karen Scida studied chemistry at the University of Texas San Antonio where she worked in the lab of Prof. Carlos Garcia. She is currently a graduate student in the group of Prof. Richard M. Crooks at the University of Texas at Austin. Her scientific interests include developing paper-based sensors as point-of-care technology and the design of bipolar electrodes for their analytical application in microfluidics.

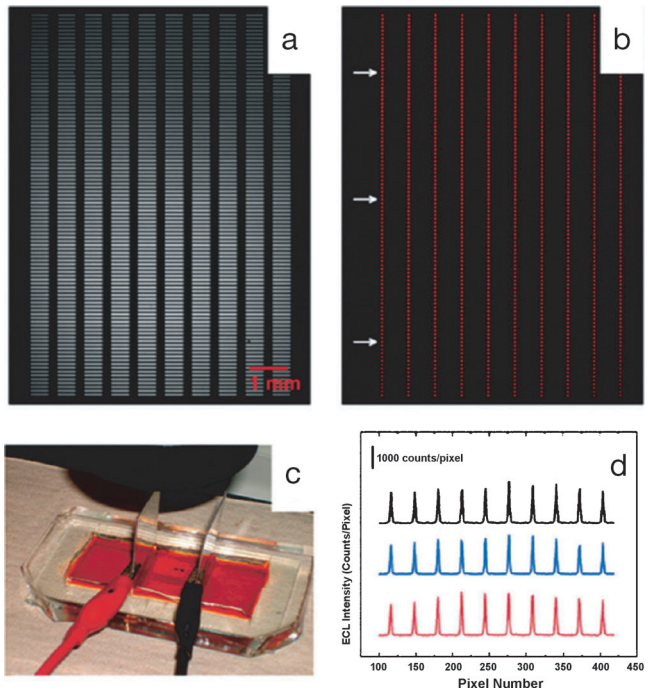

Figure 1. a) Optical micrograph of an array of 1000 Au BPEs. Each BPE is 500 μm long and 50 μm wide, and the electrodes are spaced by 50 μm vertically and 200 μm horizontally. b) Luminescence micrograph showing the ECL response of 5 mM $[Ru(bpy)_3]^{2+}$ and 25 mM tri-*n*-propylamine (TPrA) in 0.10 M phosphate buffer (pH 6.9) when $E_{tot} = 85.0$ V. c) Photograph of the bipolar electrochemical cell showing the BPE array immersed in electrolyte solution contained within a poly(dimethylsiloxane) (PDMS) reservoir. The two alligator clips are attached to stainless steel driving electrodes that span the array. d) Plot of ECL intensity vs. pixel number showing the uniformity of the ECL response over the rows of BPEs indicated by the white arrows in (b). The ECL intensity varies by no more than 10%, indicating that ΔE_{elec} is uniform over the entire array. Reprinted (adapted) with permission from Ref. [16]. Copyright 2008 American Chemical Society.

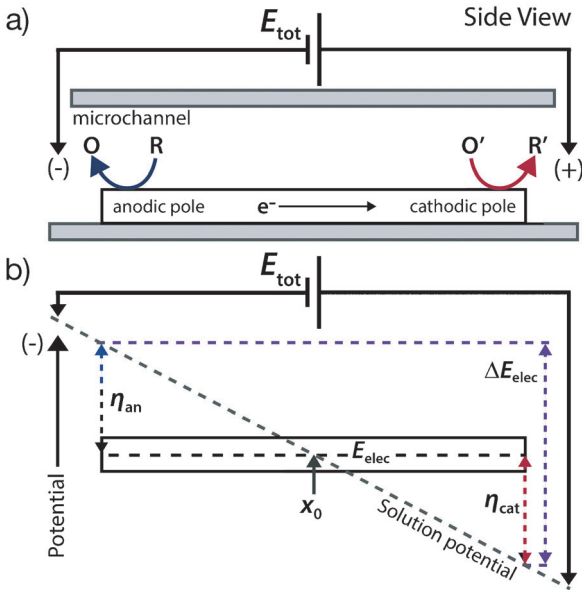

Scheme 2.

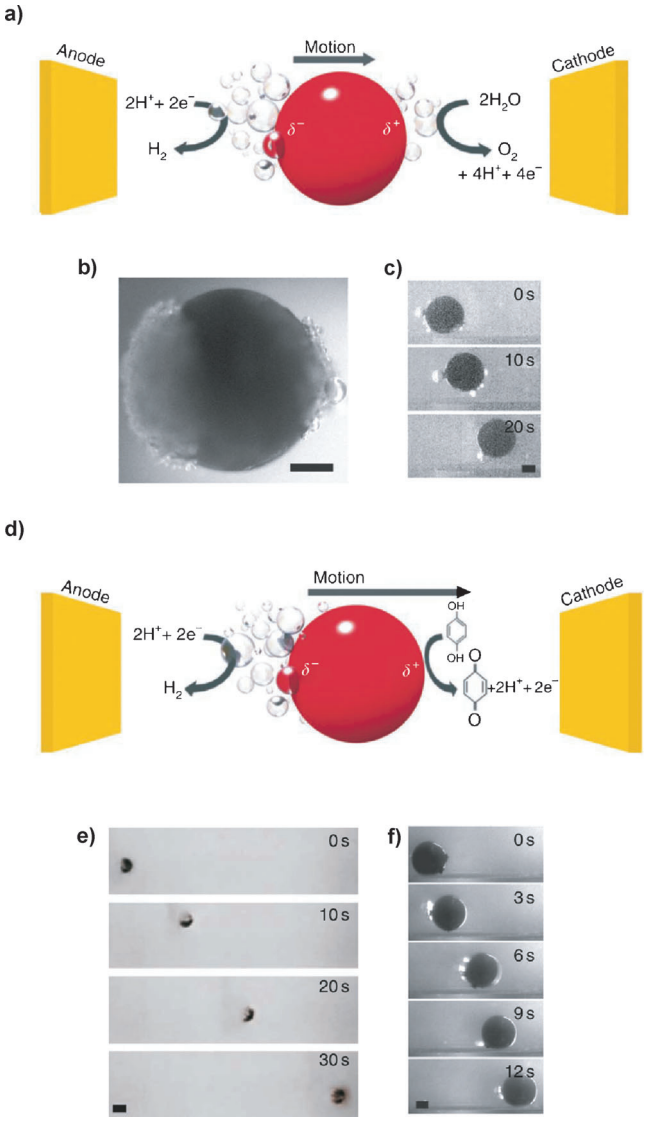

Figure 2. a) Schematic illustration of bipolar electrochemical water splitting on a conductive microbead. b) Optical micrograph of a 1 mm diameter stainless steel bead experiencing an electric field of 1.6 V mm^{-1} in 24 mM H_2SO_4. The cathodic pole is located on the left side of the bead and the scale bar indicates 250 μm. c) Motion of a 285 μm diameter glassy carbon microbead in a microchannel exposed to a 5.3 V mm^{-1} electric field in 7 mM H_2SO_4 (scale bar = 100 μm). d) Scheme showing proton reduction and hydroquinone oxidation on a BPE sphere. e) Motion of a 1 mm diameter stainless steel bead exposed to a 1.3 V mm^{-1} electric field in 24 mM HCl and 48 mM hydroquinone (scale bar = 1 mm). f) Motion of a 275 μm diameter glassy carbon microbead in a microchannel with a 4.3 V mm^{-1} electric field in 7 mM HCl and 14 mM hydroquinone (scale bar = 100 μm). Reprinted by permission from Macmillan Publishers Ltd, Nature Communications, Ref. [21], copyright 2011.

observed purple color of the indicator. In Figure 5b, a U-shaped Pt wire (BPE) has been inserted between the driving electrodes, and the change in color of the indicator demonstrates that water electrolysis occurs at its ends, even though it is not in direct electrical contact with the power supply. Moreover, the relative positions of the colors reveal the poles of the BPE are oriented in the opposite polarity of the driving electrodes.

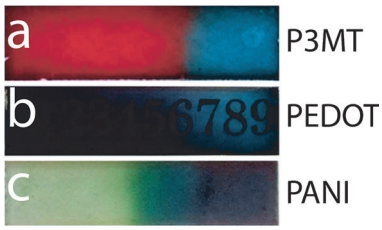

Figure 3. Gradient doping of conducting polymers. a) Poly(3-methylthiophene) (P3MT), b) poly(3,4-ethylenedioxythiophene) (PEDOT), and c) poly(aniline) (PANI). Adapted with permission from Ref. [25]. Copyright 2011 American Chemical Society.

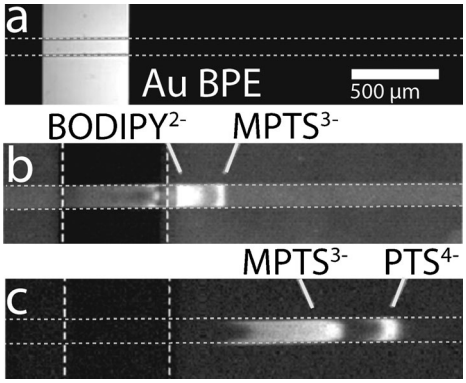

Figure 4. a) Optical micrograph of a 500 µm long Au BPE in a microfluidic channel. b) Fluorescence micrograph demonstrating simultaneous enrichment and separation of the anionic tracers 4,4-difluoro-1,3,5,7,8-pentamethyl-4-bora-3*a*,4*a*-diaza-*s*-indacene-2,6-disulfonic acid ($BODIPY^{2-}$) and 8-methoxypyrene-1,3,6-trisulfonic acid ($MPTS^{3-}$) 200 s after application of $E_{tot} = 40$ V. The white dashed lines indicate the edges of the BPE, and the gray dotted lines indicate the walls of the microchannel. (c) Fluorescence micrographs showing the enrichment and separation of $MPTS^{3-}$ and 1,3,6,8-pyrene tetrasulfonic acid (PTS^{4-}) 400 s after the application of $E_{tot} = 60$ V. Adapted with permission from Ref. [26]. Copyright 2009 American Chemical Society.

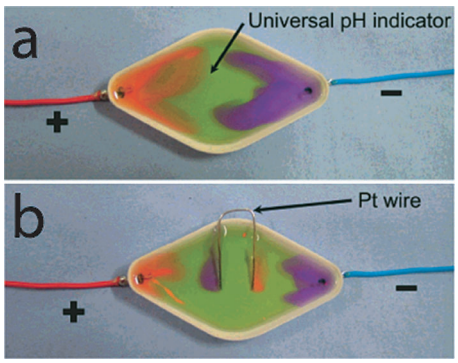

Figure 5. a) A plastic weighing boat outfitted with two Pt driving electrodes embedded in its walls and filled with a universal pH indicator solution. 30 V was applied between the two driving electrodes and the indicator solution shows the changes in local pH due to the water oxidation (left) and water reduction (right). b) When a U-shaped Pt wire is added to the weighing boat it acts as a BPE, and faradaic reactions occur at its surface. The positive driving electrode (red) induces a cathode at the nearest pole of the BPE and the negative driving electrode (blue) induces an anode. Adapted with permission from Ref. [45]. Copyright 2001 American Chemical Society.

2.2. Potential Differences in Bipolar Electrochemistry

Cells for carrying out bipolar electrochemistry can be configured to accommodate a range of applications from preparative-scale electrosynthesis to microanalysis. For example, Scheme 2a is an illustration showing a simple microscale cell design used by our group. In this case, a BPE, or an array consisting of multiple BPEs, is embedded within a microfluidic channel that has a height of tens of microns, a width of hundreds of microns, and a length of perhaps a centimeter. Potential contaminants electrogenerated at the driving electrodes do not interfere with the BPE in this design, because of the macroscale length of the channel.

The voltage applied between the two driving electrodes (E_{tot}) results in an electric field in solution that causes the BPE to float to an equilibrium potential (E_{elec}) that depends on its position in the field and the composition of the electrolyte solution. Because the electrode is a conductor, its potential (E_{elec}) is the same (or nearly so) everywhere on its surface. However, the interfacial potential difference between the BPE and the solution varies along its length due to the presence of an electric field in solution. It is these anodic and cathodic overpotentials,[36] η_{an} and η_{cat}, respectively, that drive electrochemical reactions at the poles of a BPE. Scheme 2b shows that the magnitudes of the overpotentials depend on just two experimental variables: the magnitude of E_{tot} and the length of the BPE. The location on the BPE that defines the boundary between its two poles, and therefore itself has zero overpotential with respect to the solution, is defined as x_0. Although x_0 is represented as being at the center of the BPE in Scheme 2b, its actual location depends on the nature of the faradaic processes occurring at the poles.[36]

As mentioned earlier, the magnitudes of the overpotentials vary along the length of the BPEs, with the highest overpotentials occurring at its extremities. This is in contrast to the working electrode in a traditional three-electrode cell configuration, wherein the interfacial potential difference is generally considered to be uniform (although this depends on how the cell is designed, the placement of the three electrodes relative to one another, and the resistivity of the electrolyte solution).[46] In either case, however, it is this interfacial potential difference that drives electrochemical reactions.[47] Importantly, the non-uniformity of the interfacial potential differences along the length of a BPE can be quite beneficial. For example, as we will show later, it can be used to simultaneously drive reactions at different rates or to synthesize materials and thin films having a graded composition or density.

2.3. Controlling the Electric Field and Current Paths

The electric field that powers bipolar electrochemistry is typically applied by a pair (or more) of driving electrodes, which can be metallic (e.g., Au, Ag, Pt, or stainless steel), carbonaceous (e.g., glassy carbon or graphite), or nonpolarizable (e.g., Ag/AgCl reference electrode). The nature of the electric field formed between the driving electrodes depends on the cell geometry and the conductivity of the electrolyte

solution. In some cases a linear electric field is generated by restricting the cross-sectional area of the solution between the driving electrodes, thereby increasing its resistance. This can be achieved by embedding the BPE in a microchannel having a small cross-sectional area (e.g., Scheme 2a) or by limiting the volume of electrolyte solution over a BPE in an open channel. We,[36,48] along with Duval and co-workers, have discussed many of the parameters that control bipolar electrochemical processes.[47,49–53] As alluded to earlier, these parameters include E_{tot}, the distance separating the driving electrodes, $l_{channel}$, and the length of the BPE, l_{elec}. The fraction of E_{tot} that is dropped over a BPE, which we refer to as ΔE_{elec}, can be estimated using Equation (1).[34,47,48]

$$\Delta E_{elec} = E_{tot}\left(\frac{l_{elec}}{l_{channel}}\right) \quad (1)$$

The value of ΔE_{elec} is a critical parameter for analyzing electrochemical processes at BPEs. The simple relationship expressed in Equation (1) incorporates a number of assumptions that may be possible to ignore for a particular system, but not others. For example, it assumes that an active BPE does not significantly affect the electric field in the solution, which is often not the case.

The foregoing point can be understood in terms of the equivalent circuits shown in Scheme 3, which are reasonably good approximations of the resistances present in the type of cell shown in Scheme 2a. In the absence of a BPE, the current flowing between the driving electrodes is entirely ionic (Scheme 3a).[54] The magnitude of the ionic current moving through the electrolyte is then governed by the magnitude of the applied potential (E_{tot}) and the resistance of the solution (R_S). When faradaic reactions occur at a BPE, a second path for current, in the form of electrons moving through the BPE, is available (Scheme 3b). We now define the parameter R_{elec}, which is the total resistance to electronic current posed by the BPE, hence, incorporating the charge transfer resistance (R_{ct})[54] and relevant aspects of mass transfer. If the resistance of the solution above the BPE (R_{S2}) is much lower than R_{elec}, then most of the current in the cell passes through the solution rather than the BPE. In this case, the electric field is not significantly perturbed by the BPE. However, when $R_{S2} >$ R_{elec}, which can be achieved by lowering the concentration of the electrolyte, substantial current flows through the BPE. This can cause either an increase or decrease in the local electric field strength in solution, which is proportional to $i_{tot}R_{S2}$ (i_{tot} is the total current flowing in the cell), thus resulting in a nonlinear electric field in the solution above the BPE. Duval and co-workers call this effect faradaic depolarization, and its magnitude depends on the strength of the electric field, the concentration of the supporting electrolyte, and the electrochemical properties of the electroactive species in the system.[49–53] It is also important to note that Equation (1) does not account for any potential dropping at the driving electrodes. The fractional loss of E_{tot} within the electrochemical double layers can, under some circumstances, be substantial.[36] Other electrochemical process can also mitigate Equation (1), but these are far more minor than the two discussed here and are, therefore, beyond the scope of this Review.

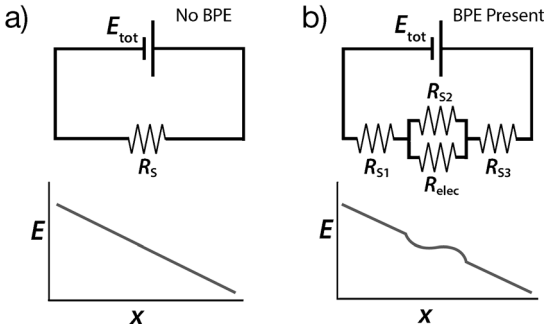

Scheme 3.

2.4. Open and Closed BPEs

The majority of this Review focuses on the use of "open" BPEs, where current can flow through both the electrolyte and the BPE. As discussed in Section 2.3, these types of devices are defined by the existence of two possible current paths: electronic and ionic. However, several interesting reports describe the use of "closed" BPEs (Scheme 4a).[55–57] In a closed BPE system, the solutions contacting the BPE anode and cathode are physically separated from one another, and the only current path between the two half cells is through a BPE (Scheme 4b).

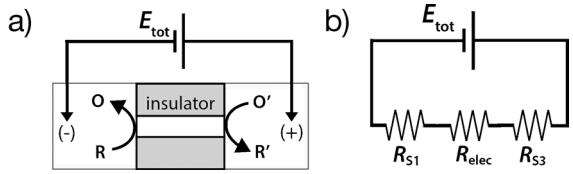

Scheme 4.

One very interesting example of closed BPEs was recently demonstrated by Zhang and co-workers.[58,59] They showed that certain types of carbon microfiber electrodes, which are commonly used in several subfields of bioelectrochemistry, actually function as closed BPEs. This was an important discovery, because it accounts for numerous measurement artifacts that have been observed over the last 30 years.

2.5. Split and Continuous BPEs

Most bipolar electrodes are continuous, meaning that the electrode is comprised of a single conductor like that shown in Scheme 1. However, it is also possible to connect two or more separate electrodes to create a BPE. We call these "split"

BPEs, and they are particularly useful because the poles can be connected to an ammeter or voltmeter exterior to the fluidic space. This means that the current and voltage can be measured in situ. Split BPEs will be discussed in greater detail in Sections 4.2 and 5.3.

With this fundamental background, we now turn to a discussion of several interesting applications of bipolar electrochemistry. These include the selective preparation of unique materials, the creation of BPE-based sensing platforms, the enrichment of charged molecules, and the development of electrochemically powered micro- and nanomotors. We also provide an outlook for the future of BPEs as a flexible platform for probing and manipulating chemical systems.

3. Materials Preparation and Fabrication

Bipolar electrochemistry is a versatile approach that simplifies some of the complications associated with micro- and nanofabrication. In most cases, where the primary focus is electrodissolution and/or electrodeposition of materials at the poles of BPEs, the only requirement is the application of a driving voltage. The inherent advantage of bipolar electrochemistry is that many electrodes can be modified simultaneously without a direct electrical connection. By carefully selecting the experimental parameters, electrochemical reactions can be easily controlled. As such, bipolar electrochemistry has advantages over other techniques, because it is capable of producing gradients of electrodeposited materials as well as providing a means for site-selective deposition.

3.1. Wire Formation

A direct electrical connection between physically separated BPEs can be achieved using bipolar electrochemistry. Scheme 5a shows that if ΔE_{elec} is sufficiently high, then a metallic BPE can undergo electrodissolution at its anodic pole, thereby producing metal cations that can subsequently be electrodeposited on the cathodic pole of a second, nearby BPE. In a very early demonstration of this principle, Bradley and co-workers showed that two separated Cu particles could be brought into electrical contact by directional growth of Cu microwires (Figure 6).[60–65] Initially, the faradaic processes at both particles were electrodissolution of Cu at the anodic poles and water reduction at the cathodic poles (Scheme 5a). However, when electrogenerated Cu^{2+} reached the cathodic pole of the particle to the left, electrodeposition of Cu competed with water reduction and the formation of Cu dendrites was observed (Figure 6a). The important point is that the two objects were electrically connected (Figure 6b) without using photolithographic methods and without having to make an ohmic contact to either object. In a related experiment, Bradley et al. were able to obtain electrical contacts between a Si semiconductor plate sandwiched by two Cu rings.[66] By switching the direction of the electric field, wire connections were formed between each Cu ring and the Si plate in the middle, leading to structures that functioned as

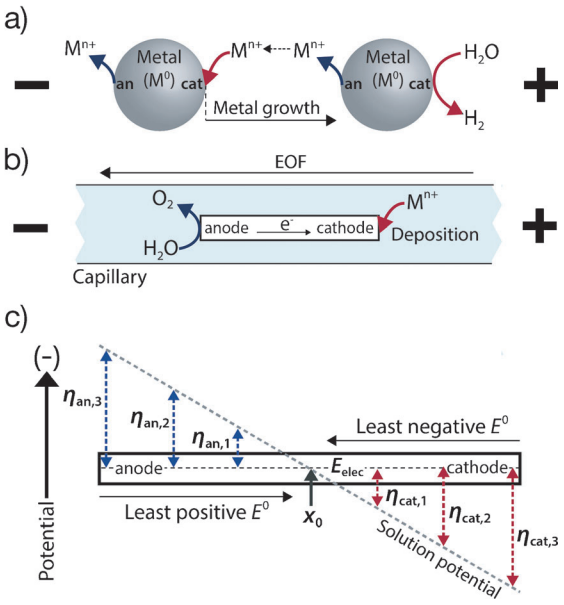

Scheme 5.

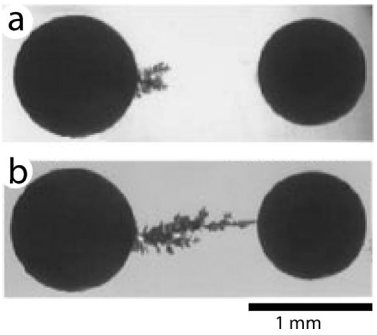

Figure 6. Formation of Cu wires between Cu particles by simultaneous electrodeposition and electrodissolution *via* bipolar electrochemistry. Two ca. 1 mm-diameter Cu particles were suspended in an aqueous solution and oriented between a pair of Pt driving electrodes. Cu deposits formed after a) 10 s and b) 29 s with an applied potential bias of 45.5 V. Adapted with permission from Macmillan Publishers Ltd, Nature, Ref. [60], copyright 1997.

diodes. Because many such contacts can be established simultaneously, and because the method easily translates to the nanoscale, it seems reasonable to expect that this approach will eventually find commercial applications.

Bradley and co-workers also used bipolar electrochemistry to prepare heterogeneous catalysts. For example, they investigated the electrodeposition of Pd onto graphite particles embedded within paper substrates.[67] They also electrodeposited Pd onto carbon nanotubes (CNTs) and nanofiber tips.[68] These are interesting examples of nanoscale modification of carbon materials and mark a novel method for preparing heterogeneous catalysts.

3.2. Asymmetric Modification of Materials

Kuhn and co-workers have greatly expanded upon the pioneering electrodeposition studies of Bradley's group. For example, they showed that electrochemistry could be carried out on nanoscale BPEs. This is a significant advance because, according to Equation (1), bipolar electrodeposition onto nanoscale objects requires very high electric fields to achieve a sufficient ΔE_{elec} to drive electrochemical reactions. Kuhn solved this problem by using a capillary electrophoresis (CE) setup to apply the field. The technique is called capillary assisted bipolar electrodeposition (CABED). The experimental arrangement consists of a small-bore capillary filled with an aqueous solution containing the CNTs and a salt of the metal to be deposited onto them (Scheme 5b).[69] Just as in CE, the ends of this capillary are placed into compartments housing driving electrodes connected to a high voltage power supply. The resulting electric field leads to electroosmotic flow (EOF) from the anodic to the cathodic compartments. In one example from Kuhn's group, mobile CNTs acted as the BPEs, and as they moved toward the cathodic compartment, water was oxidized at their anodic poles and Au^{3+} was reduced to Au^0 at their cathodic poles. This resulted in electrodeposition of Au at just one end of the CNTs (Figure 7). Other metals, including Cu and Ni, were also

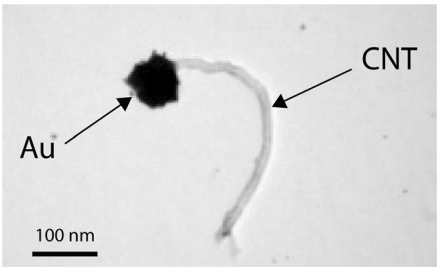

Figure 7. Transmission electron micrograph of a 500 nm CNT and the asymmetric deposition of Au via CABED. The CNTs were placed in a 45 cm long capillary containing aqueous 1.0 mM $HAuCl_4$. Upon the application of 30 kV, Au deposited at the cathodic pole of the CNT. Adapted with permission from Ref. [69]. Copyright 2008 American Chemical Society.

electrodeposited using the same method, with the latter composite having magnetic properties.[70] Non-metallic materials, such as conductive polymers, can also be deposited using CABED.[71] For example, Janus-type objects were created by oxidizing pyrrole at one end of a CNT, to produce poly(pyrrole), and reducing Cu^{2+} at the other end.

While Kuhn's initial studies focused on capillary-based techniques, they showed that similar results could be achieved in simpler bipolar electrochemical cells. Specifically, the limitation on the number of particles that could be modified in the capillary was alleviated by a clever cell design where a pair of polymer or sintered glass membranes were employed to separate the BPEs and reactants from the driving electrodes and an inert electrolyte solution.[72] They demonstrated the utility of this approach by electrodepositing Cu,[73] Au,[72] and Pt[72] onto dispersions of carbon microtubes and glassy carbon beads. Kuhn and co-workers also used this type of cell to modify carbon microbeads using an indirect electrochemical approach in which a pH gradient was generated at the poles of a BPE to selectively precipitate inorganic and polymeric layers.[74] For example, silica, TiO_2, and electrophoretic deposition paints were prepared site-selectively using this method. Kuhn and co-workers have also demonstrated the bipolar electrodeposition of Prussian blue on graphite rods, which can be used to generate luminol chemiluminescence.[75]

Bipolar electrochemistry can also be combined with other methods to achieve interesting results. For instance, Nelson and co-workers developed a technique, which they call floating-electrode dielectrophoresis, for BPE-aided dielectrophoretic assembly of CNTs.[76] Here, BPEs smooth the electric field and allow for more precise and predictable deposition of CNTs at desired locations.

3.3. Generation of Compositional Gradients

As mentioned earlier, the highest overpotentials are generated at the outermost edges of a BPE and they gradually decrease until reaching x_0 (Scheme 5c). It is possible to take advantage of this property of BPEs to prepare gradients of materials. For example, Björefors and co-workers showed that gradients of thiol-based self-assembled monolayers (SAMs) could be prepared by controlled potential desorption or deposition onto Au BPEs.[77] In this case, the surface density of thiols is controlled by the variable interfacial potential difference along the BPE (Scheme 5c). The same group used surface plasmon resonance to show that electrochemical gradients of $[Fe(CN)_6]^{4-}$ and $[Fe(CN)_6]^{3-}$ could be prepared in a solution in contact with a Au BPE (Figure 8).

When two or more different electroactive materials having different standard potentials ($E°$) are present in solution, a compositional gradient can be formed along the length of a BPE. In this case, the materials having the least

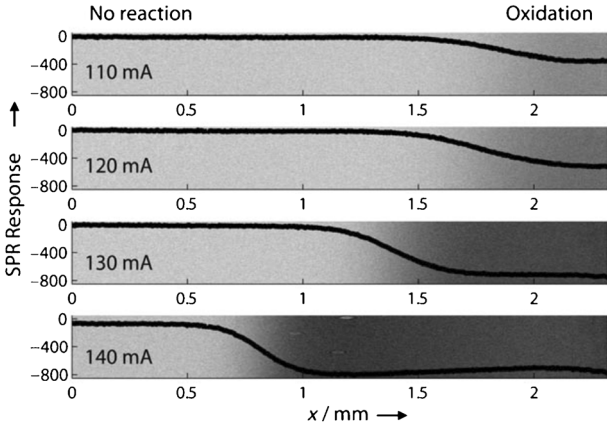

Figure 8. Surface plasmon resonance image of the gradient oxidation of $[Fe(CN)_6]^{4-}$ to $[Fe(CN)_6]^{3-}$ at the anodic pole of a BPE as a function of the indicated total currents. The voltage was applied through a 200 mM $[Fe(CN)_6]^{4-}$ solution via two stainless steel driving electrodes.

negative $E°$ (requiring the least overpotential) are deposited closest to x_0, while those having the most negative $E°$ (requiring the highest overpotential) are only deposited at the ends of the BPE (Scheme 5c). Shannon and Ramakrishnan demonstrated this principle by electrodepositing a compositional gradient of CdS on a Au BPE.[78] The composition of the gradient was analyzed by surface enhanced Raman spectroscopy and found to be consistent with the $E°$ values required to deposit the individual materials. In other words, the gradient was well-defined and predictable. The same technique was used to synthesize gradients of Ag-Au alloys on stainless steel BPEs.[79]

Inagi, Fuchigami, and co-workers showed that conductivity gradients of conductive polymers can be prepared on BPEs by position-dependent doping and undoping in nonaqueous solvents.[24,25,80–82] For instance, a poly(3-methylthiophene) (P3MT) film on an ITO support was anodically doped with PF_6^-, changing its color from dark red to blue (Figure 3a).[24] Other dopants (e.g., Cl^-) and conductive polymers (e.g., poly(aniline) and poly(3,4-ethylenethiophene)) were manipulated in a similar way,[25] more localized doping was achieved by manipulating the experimental set-up,[81] and electro-click reactions were also proposed for selective modification of electrode surfaces.[82]

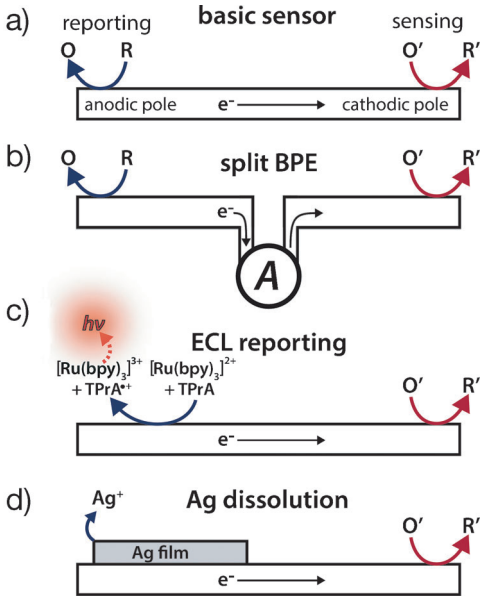

Scheme 6.

4. Sensing and Screening Applications

4.1. Principles of BPE-based Sensing

BPEs have only recently been used as electroanalytical sensors, probably because it is not easy to directly measure the current flowing through them. However, our group recently solved this problem. Consequently, the advantages of using BPEs for sensing and screening applications have become more compelling. Within the context of sensing and screening, these advantages include: 1) no direct electrical connection is required; 2) many electrodes can be controlled simultaneously with a single DC power supply; 3) the sensing electrodes can have micron-scale, or even nanoscale, dimensions.

The basic operating principle of BPE sensing and screening devices relies on electrical coupling between the sensing and the reporting poles (the reporting pole is the end of the BPE signaling the state of the sensing pole). In other words, the current passing through the two poles of the BPE must be equal (i.e., $i_{cat} = -i_{an}$). For example, and as shown in Scheme 6a, if the sensing reaction is an electrochemical reduction, then the electrons required at the cathodic pole originate from a proportional oxidative reporting reaction at the anodic pole. In the absence of the analytical target species, no oxidation occurs. Most reporting reactions that have been discussed in the literature are oxidations that generate an easily observable optical signal at the anodic pole of a BPE. Optical readouts include ECL, fluorescence, and anodic dissolution (or change in refractive index) of a metal film. The advantage of these approaches is that they are easily implemented in parallel and are thus amenable to simultaneous readout of large arrays of BPEs. When employing these arrays, it is important to consider that sensing and screening experiments typically require each electrode to act independently of others, and therefore the amount of diffusion layer overlap between electrodes and the extent of faradaic depolarization should be minimized.

4.2. Amperometric Detection using Split Microband BPEs

It is also possible to directly measure the current passing through a BPE by inserting an ammeter between its poles (Scheme 6b). This method is useful for calibrating optical signals for a small number of BPEs, but it is impractical for large arrays because an ammeter would be required for each electrode. An early demonstration of directly measuring the current flowing through a BPE was introduced by Nyholm and Klett, who used BPEs for amperometric detection in CE.[83] For this purpose, they used the split BPE configuration shown in Scheme 6b, which consists of two separated poles connected external to the capillary with an ammeter. By taking advantage of the electric field inherent to CE, this approach avoids the need for a potentiostat. Note, this high field is a nuisance when one tries to integrate traditional three-electrode electrochemical detection into CE.[84] The authors demonstrated that a split BPE produces results similar to those obtained using cyclic voltammetry. Nyholm and co-workers later expanded this work to include an array of 20 Au microbands so that analytes with different $E°$ values could be detected simultaneously.[85]

4.3. Sensing and Reporting by ECL at a Single BPE Pole

To avoid making a direct electrical contact to the BPE, Manz and co-workers introduced ECL as an optical signal transduction method (Scheme 6c).[45] Briefly, ECL occurs when an excited state molecule, generated from a series of

charge-transfer reactions, relaxes to the ground state and emits a photon.[86] ECL is highly sensitive, with near zero-background signal, because no excitation light source is required to drive it. One of the most effective and widely used ECL reactions involves the co-oxidation of tris(bipyridine)ruthenium(II) ($[Ru(bpy)_3]^{2+}$) and tri-*n*-propylamine (TPrA). Manz and co-workers used this type of ECL reaction to detect $[Ru(phen)_3]^{2+}$ and $[Ru(bpy)_3]^{2+}$ following electrophoretic separation. In this case, TPrA was present in the separation column, and the electric field required for CE separations energized the BPE. When both detection and readout occur at the same pole of the BPE, as in this example, then the accessible analytes are limited to species that participate or compete with the ECL-producing reaction. A competition reaction was recently demonstrated in which mRNA sequences associated with breast cancer cells displaced a second strand labeled with a $[Ru(bpy)_3]^{2+}$-laden silica particle resulting in a reduction in ECL intensity.[87]

4.4. Electrically Coupled Sensing using ECL

Our group introduced a sensing scheme in which the reporting and sensing reactions occur on different poles. The important innovation here is that the sensing and reporting poles are decoupled, but their electrochemical relationship is preserved via conservation of charge (Scheme 6). This new approach eliminated the previous requirement that analytes be capable of direct participation in the ECL reaction sequence, and hence opened the door to BPE sensing of a wide variety of analytes.

In our initial study, we showed that the detection of benzyl viologen (BV^{2+}) at the BPE cathode was electrically coupled to ECL emission occurring at the anode (Scheme 6c). Moreover, the effect of electrode length and geometry on ECL emission were investigated.[34] With Duval's work as a foundation, we described a semi-empirical approach for predicting E_{elec}, in addition to ΔE_{elec} as a function of E_{tot}, and we showed that the intensity of ECL emission can be directly correlated to the magnitude of current flowing through the BPE.[36] During a sensing or screening experiment using BPEs as illustrated in Scheme 6, which we refer to as "open" BPEs, it is critical that each electrode experiences a uniform electric field. As alluded to earlier, this means that only a small fraction of the total current, typically less than 1%, is permitted to pass through the BPE with the remainder traversing the solution as an ionic flux (Scheme 3b).[36] Closed BPEs do not have this requirement because the only path for current flow between driving electrodes is via electron transfer through the BPEs (Scheme 4).

On the basis of these simple operating principles, BPE sensors have been employed to detect myriad analytes. For example, our group demonstrated a DNA sensor with ECL readout following a design similar to that shown in Scheme 6c, except the cathodic pole of a Au BPE was modified with a thiol-terminated probe single-stranded DNA (ssDNA) sequence.[35] In a control experiment, with $E_{tot} = 22.0$ V, no ECL was observed because ΔE_{elec} was insufficient to drive significant faradaic reactions at the modified Au BPE. However, when the target ssDNA labeled with a Pt nanoparticle (NP) hybridized with the electrode, $E_{tot} = 22.0$ V was sufficient to drive the oxygen reduction reaction (ORR) at the Pt NP surface. The lowering of the required η_{cat}, and thus ΔE_{elec}, by the Pt catalyst then activated ECL emission at the anode. This experiment also clearly demonstrated a basic principle of many BPE sensing platforms: the sensing reaction must facilitate or catalyze a reaction to enhance the current flowing through the BPE.

As previously mentioned, one of the main virtues of bipolar electrochemistry is that many BPEs can be driven simultaneously using a single power supply and two driving electrodes. Figure 1a is an optical micrograph of a device that incorporates 1000 BPEs.[16] When a sufficiently high E_{tot} is applied through the two driving electrodes spanning the array, red ECL emission is observed at the anode of each of the electrodes (Figure 1b). As shown in Figure 1c, the configuration of this device is extremely simple. The most important design rule for large arrays of this sort is that the potential dropped over each electrode (ΔE_{elec}) be the same. In the present case, this is demonstrated by the remarkable uniformity of the ECL line scans shown in Figure 1d. In this particular experiment, no sensing chemistry was placed on the cathodic poles of the BPEs, but clearly this can be accomplished using a robotic spotter, as we will discuss later in Section 4.6, to yield massively parallel sensing arrays.

In some cases, the solution conditions required for sensing and reporting reactions may be incompatible with one-another, and hence it is necessary to place the anodic and cathodic poles of the electrodes into spatially isolated compartments. To address this requirement, we developed a bipolar electrochemical cell in which a BPE, or multiple BPEs, span two microchannels.[43] When the same E_{tot} is applied across the two channels, the sensing and reporting reactions are electrically coupled through the BPE but remain otherwise separated. This approach has been used to follow ECL emission coupled to the reduction of $[Fe(CN)_6]^{3-}$, which can be used for the indirect detection of glycated hemoglobin.[43] Chen and co-workers recently used a similar two-channel design to detect prostate-specific antigen (PSA). In their approach, PSA guides the deposition of Ag NPs to the space between two microbands. Eventually the two microbands become electrically connected, and the resulting BPE has sufficient length to generated ECL at the applied value of E_{tot}.[88]

Interestingly, new functionality has been introduced to ECL reporting by changing either the electrochemical cell or the shape of the BPE. In the former case, we showed that when a single BPE is present at the intersection of two microchannels, four driving electrodes can be used to control the electric field in such a way that electrochemical reactions can be localized at specific points on the BPE surface.[40] In the latter case, the shape of the BPE was changed from a simple rectangle to a triangle. A single triangle acts just like an array of individual BPEs having different lengths, which means that each location on the edge of a triangular BPE experiences a different overpotential. Hence, a single luminescence micrograph can be used to extract kinetic information using a technique we call "snapshot voltammetry".[39] We

have also shown that multiple channels and BPEs can be configured to yield logic functions like NOR, OR, and NAND with optical readout.[37,89] These could eventually be useful for sensing and signaling applications. Foret, Manz, and co-workers recently demonstrated that floating Au platelets can act as BPEs in a CE separation, where ECL might be used to follow a cathodic sensing reaction.[90] The important result is that the platelets are easily replaced because they move in the separation volume.

4.5. Detection using the Anodic Dissolution of a Metal Film

In addition to ECL readout, our group has pioneered the use of metal film electrodissolution as a reporting reaction for bipolar electrochemistry.[38] When E_{tot} is applied, the electrodissolution of thermally deposited Ag is electrically coupled to a reduction reaction occurring at the cathodic pole of the BPE (Scheme 6d). Because η_{an} is highest at the extreme edge of the BPE anode, Ag first begins to dissolve at the distal edge of the electrode and then continues to dissolve toward x_0. The dissolution will continue until it reaches a critical point, where ΔE_{elec} cannot drive the two types of faradaic processes. This approach has a number of advantages over the ECL signaling method. First, it eliminates the need for detection of light, because the change in length of the electrode can be read with the naked eye. Second, it eliminates the need for solution-phase reagents like $[Ru(bpy)_3]^{2+}$. Third, the amount of charge stored in the Ag as a function of its length depends only on the thickness of the film, and therefore a very broad dynamic range of sensitivities is available for sensing applications. Fourth, Ag dissolution is associated with a single redox process, whereas ECL relies on two redox processes which can compromise the limit of detection for sensing applications.[36]

We demonstrated the idea of using the Ag electrodissolution reaction for chemical sensing by immobilizing a probe ssDNA sequence on the cathodic pole of a BPE.[38] When a target sequence labeled with horseradish peroxidase (HRP) hybridized to the probe, the HRP catalyzed the reduction of H_2O_2 to water via a mediator. The presence of the mediator, and hence the ssDNA target, was then signaled by a change in the length of the Ag thin film at the anodic pole of the BPE. In the absence of the target, no change was observed.

Interestingly, a BPE can be activated without any external power source. This type of device, which is shown in Figure 9a, is powered by a phenomenon called streaming potential, which is essentially the opposite of electroosmosis because it is initiated by simply pushing an electrolyte solution through a microchannel having charged walls.[41] Streaming potentials used for the experiment shown in Figure 9 resulted from the movement of counterions in the electrical double layer at the interface between the electrolyte solution and the charged walls of a poly(dimethylsiloxane) (PDMS)/glass microchannel. When the resistivity of the electrolyte solution is kept high ($\approx M\Omega\,cm^{-1}$), streaming potentials of up to 8 V can be achieved. As a proof of concept, benzoquinone was detected using Ag electrodissolution as a reporting mechanism (Figure 9b,c). By eliminating the need for a power source, this type of detection scheme opens up the possibility to perform point-of-care sensing applications in resource-limited settings.

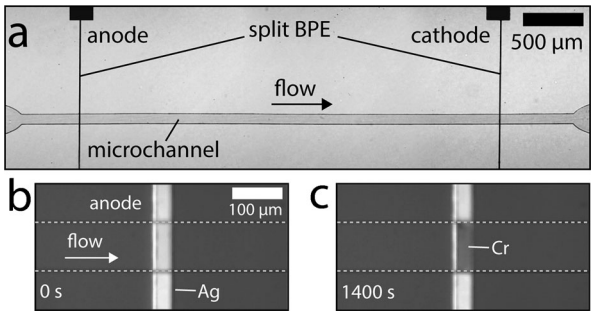

Figure 9. a) Optical micrograph of a microfluidic channel that incorporates a split BPE for streaming potential experiments. The channel was 6 mm long and the BPE consisted of two Au microbands making $l_{elec} = 4.5$ mm. b) An optical micrograph of the BPE anode, which was modified with a 20 nm thick layer of Ag over 5 nm of Cr. The channel contained an aqueous 1.0 mM benzoquinone solution. At $t = 0$ s, the two poles of the BPE were connected externally. c) After 1400 s, the Ag film was completely oxidized. Adapted with permission from Ref. [41]. Copyright 2011 American Chemical Society.

4.6. Electrocatalyst Screening

In addition to using metal film dissolution for sensing applications, it can also be used for the rapid screening of electrocatalysts. In one recent example from our group, the cathodic poles of an array of BPEs were spotted with catalyst candidates for the ORR.[42] When a voltage was applied across the array by a pair of driving electrodes, electrodissolution of Ag microbands was initiated. The key point is that the number of bands dissolved depends on the efficiency of the associated electrocatalyst. This concept is illustrated schematically in Figure 10.

This method relies on the fact that the overpotential between the BPE and the solution varies laterally along the BPE (Scheme 5c). The most effective electrocatalyst requires the lowest ΔE_{elec} for dissolution of Ag, and therefore, the overall length of the BPE associated with that catalyst will be the shortest at equilibrium. In other words, as the bands begin to dissolve, the effective length of the electrode (l_{elec}) decreases, which in turn decreases ΔE_{elec} [Eq. (1)]. The bands stop dissolving once this driving force becomes insufficient to simultaneously drive Ag oxidation and the ORR. Figure 10c shows the screening device prior to the application of E_{tot} and Figure 10d shows the result of the experiment. The readout of this device is simple: the more Ag bands that dissolve, the better the electrocatalyst. We have recently expanded and improved our BPE electrocatalyst screening platform by increasing the size of the array by an order of magnitude, changing the identity of the anodic reporter to Cr (which oxidizes near the thermodynamic potential of the ORR), and implementing piezodispensing as a method of introducing compositionally varied electrocatalyst candidates.[44] This setup was used to evaluate three bimetallic systems for the ORR: Pd-Au, Pd-Co, and Pd-W.

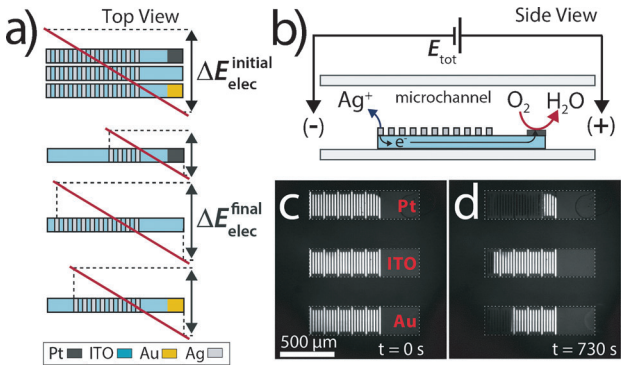

Figure 10. a) Top: schematic illustration of three BPEs having different electrocatalyst candidates for the ORR immobilized on their cathodic poles. The functional anodes of the BPEs consist of an array of 25 Ag microbands. The red line indicates the potential, which is initially uniform, dropped over each electrode. Bottom: When E_{tot} is applied and some Ag bands dissolve, the effective length of each BPE decreases. This results in a lowering of ΔE_{elec} until it reaches a value that is insufficient to drive additional faradaic reactions. b) Side view of one BPE showing the electrochemical processes at the anodic and cathodic poles. c) Optical micrograph of an array of three BPEs modified with the indicated catalyst candidates prior to application of E_{tot}. The ITO support has been outlined using the gray dashed lines. d) Optical micrograph of the same BPE array after application of E_{tot}. The change in the number of Ag microbands reveals the relative activity of each catalyst candidate. Adapted with permission from Ref. [42]. Copyright 2012 American Chemical Society.

Following our original work relating to catalyst screening using open BPEs, two interesting reports recently appeared describing similar results but using closed BPEs. In the first example, several Pt nanomaterials were dropcast onto glassy carbon electrodes that were placed into cells containing air-saturated 0.5 M H_2SO_4. The electrodes were electrically connected to Pt microdisk electrodes immersed in a solution containing the ECL reactants. Using this setup, Chen and co-workers report that the ECL at the Pt microdisks is directly correlated to the ORR occurring at the Pt catalyst candidates, which provides a simple means for high throughput screening.[91] In the second example, Zhang and co-workers introduced a method they call fluorescence enabled electrochemical microscopy (FEEM).[92] In this experiment, they prepared large arrays of micron-scale carbon-fiber (CF) BPEs, and then patterned Pt films on one side of this array using bipolar electrodeposition. During the screening experiment, the Pt-modified BPE anodes catalyzed the oxidation of H_2O_2 to O_2, while a non-fluorescent species was reduced to a fluorescent species at the BPE cathode. In regions of the array not patterned with Pt, no fluorescence was observed. This approach shows great promise for large-scale, electrochemical imaging.

5. Bipolar Electrode Focusing

5.1. Principles of BPE Focusing

Due to small sample volumes and low absolute numbers of molecules present within microfluidic devices, the detection of analytes in such systems often requires a preconcentration step prior to analysis. Our group, together with our collaborators Prof. Ulrich Tallarek and Dr. Dzmitry Hlushkou from Philipps-Universität Marburg in Germany, have shown that BPEs can be employed to address this issue by enriching charged analytes along a locally generated electric field gradient.[93] We call this method BPE focusing, and it is a member of a family of analyte enrichment techniques based on the principle of electrokinetic equilibrium. More specifically, BPE focusing is a counter-flow gradient focusing technique in which charged analytes enrich when electromigration (EM) is balanced against convection.[94]

The key to this technique involves generation of a local electric field gradient near a BPE. When a sufficiently high potential bias is applied across a microchannel having an embedded BPE (Scheme 7a), water electrolysis may proceed at the BPE poles following Equations (2) and (3), respectively.

$$2\,H_2O \rightleftharpoons O_2 + 4\,H^+ + 4\,e^- \quad (2)$$

$$2\,H_2O + 2\,e^- \rightleftharpoons H_2 + 2\,OH^- \quad (3)$$

$$TrisH^+ + OH^- \rightleftharpoons Tris + H_2O \quad (4)$$

For anionic enrichment, electrogenerated OH^- at the BPE cathode (Scheme 7b) may neutralize a positively charged buffer cation, such as the protonated form of tris(hydrox-

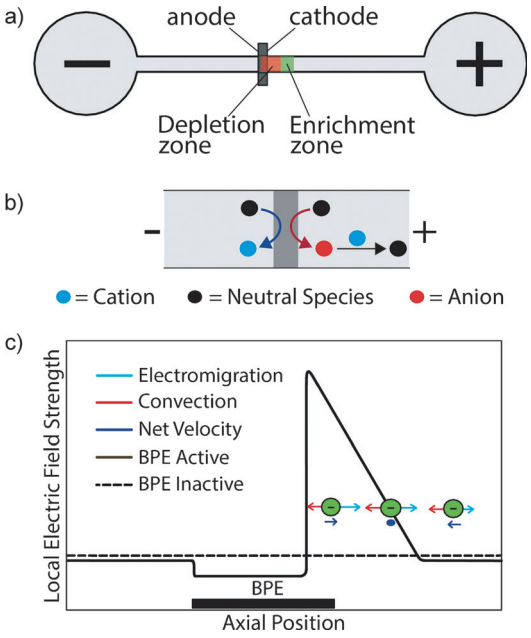

Scheme 7.

ymethyl)aminomethane ($TrisH^+$) [Eq. (4)], thereby forming an ion depletion zone near the BPE. The increased solution resistivity within the ion depletion zone causes a large proportion of E_{tot} to be dropped in this region. It is this electric field gradient that allows the local enrichment of analyte in the presence of a counter-flow.

This local electric field gradient does not appear in the systems previously discussed in this review, because in those cases the system is designed to ensure that only a small fraction of the total current passes through the BPE. However, by simply lowering the electrolyte concentration in the microchannel, most of the current can be forced through the BPE. This concept can be easily understood in terms of Scheme 3b. For enrichment experiments in a single microchannel, R_{S2} is kept high, thereby diverting the current through R_{elec}. Other groups have also reported the use of BPEs for enrichment by either generating pH gradients or non-uniform EOF.[95,96]

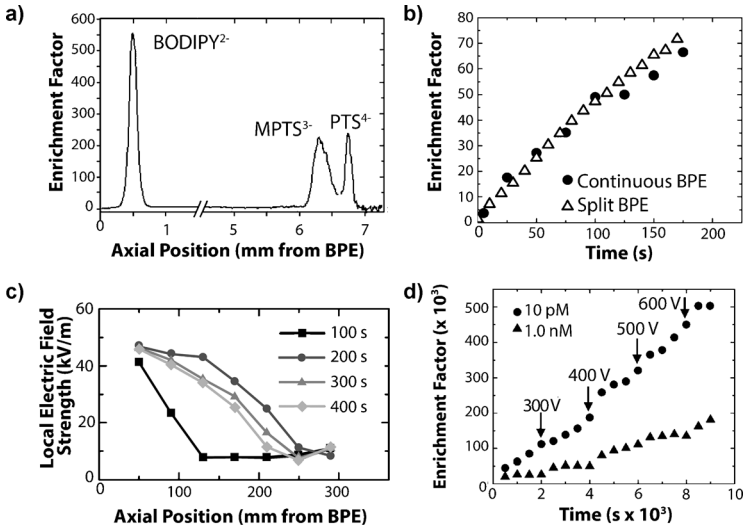

Figure 11. a) Plot of enrichment factor vs. axial distance from the BPE cathode showing the enrichment and separation of $BODIPY^{2-}$, $MPTS^{3-}$, and PTS^{4-} in 5.0 mM $TrisH^+$ with $E_{tot}=40.0$ V in a 12 mm-long, Pluronic-coated channel. Adapted with permission from Ref. [26]. Copyright 2009 American Chemical Society. b) Comparison of the enrichment factor as a function of time for $BODIPY^{2-}$ at split and continuous BPEs with $E_{tot}=35.0$ V in 5.0 mM $TrisH^+$. Adapted with permission from Ref. [27]. Copyright 2009 American Chemical Society. c) Experimentally determined local axial electric field strength as a function of position and time with $E_{tot}=35.0$ V in 5.0 mM $TrisH^+$. Adapted with permission from Ref. [28]. Copyright 2011 The Royal Society of Chemistry. d) Plot of enrichment factor vs. time for 10.0 pM (circles) and 1.0 nM (triangles) $BODIPY^{2-}$ in pH 8.1, 100 mM $TrisH^+$. Initially, $E_{tot}=200$ V, but it was periodically raised at the indicated times. Adapted with permission from Ref. [29]. Copyright 2011 American Chemical Society.

5.2. Electrokinetics and Mass Transport

The transport of charged analytes during a BPE focusing experiment is controlled by convection and EM. A cathodic EOF develops when a potential bias is applied across the negatively charged walls of a PDMS/glass microchannel. In addition to EOF, bulk solution flow can be controlled in either direction by pressure-driven flow (PDF), which is initiated by creating a solution height differential in the reservoirs at the channel ends by simply adding or removing solution.

The electrophoretic (EP) velocity of a charged analyte (u_{ep}) in an electric field is dictated by Equation (5), where μ_{ep}

$$u_{ep} = \mu_{ep} V_1 \quad (5)$$

is the EP mobility and V_1 is the local electric field strength. Consequently, as anions enter the microchannel and approach the BPE, they experience an increasing u_{ep} as the electric field strength increases. Enrichment occurs when the velocities due to EM and convection are equal in magnitude and opposite in direction (Scheme 7c). Because the location of enrichment depends on μ_{ep} [Eq. (5)], analytes having different EP mobilities may be simultaneously separated and enriched at different locations in the channel. Figure 11a shows the separation and enrichment of three negatively charged tracers having different μ_{ep} as a plot of enrichment factor (EF, ratio of the concentration in the enriched band to the initial concentration) vs. distance from the BPE.[26]

5.3. Guidelines for Enrichment

The formation and stability of the electric field gradient near a BPE has been investigated in several fundamental studies. For example, we measured the current flowing through a split BPE to show that a significant change to the local electric field gradient results only after a large percentage (ca. 80%) of the total current passes through the BPE (Scheme 3b).[27] In other words, only when there is a significant degree of faradaic depolarization is a locally enhanced electric field observed. There are three additional aspects of BPE focusing worth mentioning here. First, split and continuous BPEs lead to local electric fields having similar characteristics, and hence result in the same degree of enrichment (Figure 11b).[27] Second, an array of microband electrodes embedded within a microchannel can be used to directly measure the axial electric field, and this type of experiment (Figure 11c) confirms the shape of the local electric field illustrated in Scheme 7c. Third, the electric field gradient has been shown to be stable for > 2.5 h.[28,29]

To better understand the interplay between forces necessary for BPE focusing, our collaborators have performed simulations,[26–28,93,97,98] and we have used these to optimize the extent and rate of enrichment. As a general guiding principle, steeper electric field gradients lead to more compact and highly enriched bands, although shallower gradients are better for separating mixtures of charged analytes. Steeper gradients are achieved by using higher ionic strength buffers, because this leads to a larger difference in electrolyte concentration between the ion depletion zone and the bulk concentration of the buffer. As discussed earlier, however,

lowering R_S decreases the current flowing through the BPE, which adversely affects the ion depletion zone. Fortunately, this seeming contradiction can be resolved by reducing the cross-sectional area of the fluidic channel.[29] The bottom line is that high buffer concentrations and small cross-sectional areas lead to EFs of >500000 (Figure 11 d).[29]

Another important fact about BPE focusing is that lower initial analyte concentrations typically lead to higher EFs. This is because enrichment of the analyte occurs within the ion depletion layer, and because the analyte itself is a charge carrier it increases the local conductivity of the solution. As the concentration of the enriched band approaches that of the background buffer, enrichment ceases.[97]

Although many analytical methods have been described in the literature for enriching anions, far fewer are available for cations. This is because cationic enrichment often requires an anodic EOF. BPE focusing can be adapted to enrich cations by coating the microchannel walls with a positively charged polymer, thereby reversing the direction of EOF from cathodic to anodic.[33] In addition, the positively charged buffer used for anion enrichment must be replaced with one that is negatively charged such as HCO_3^-. The latter is neutralized by H^+ produced at the BPE anode, and therefore enrichment of cations occurs at the anodic pole of the BPE, rather than at the cathodic pole.[33]

5.4. Applications of BPE Focusing

Beyond enrichment and separation, we have also shown that manipulating the local electric field gradient with a BPE is useful for a variety of other applications.[30] For example, it can be used to concentrate and direct the flow of charged analytes.[32] As previously discussed, enrichment occurs when EM balances convection. This means that the forward movement of an analyte ceases when its EP velocity is greater than or equal to the opposing convective velocity. Using these principles, we have demonstrated the controlled transport and selective delivery of two charged analytes by employing a microfluidic design having two microband BPEs embedded near the split of a Y-shaped microchannel (Scheme 8). In this configuration, the BPEs act as on/off switches for an electric field gradient. Specifically, when both BPEs are activated using an external switch, the local electric field strength is high and the analytes enrich and separate in the main channel (Scheme 8 a) as discussed earlier in the context of Figure 11 a. Then, when one BPE is disconnected and the PDF is increased from right to left (Scheme 8 b), both enriched bands move toward the intersection. By carefully controlling when the gating BPEs are active, the anionic fluorescent tracer closest to the intersection ($BODIPY^{2-}$, represented by the black ball) is delivered into the lower secondary channel. This occurs because the local electric field in this region of the channel has been lowered, leading to a lower EP velocity and the dominance of PDF. After this delivery, the first BPE is reconnected and the second one is disconnected, thus allowing the other fluorescent tracer ($MPTS^{3-}$), represented by the gray ball, to be delivered into the upper secondary channel by PDF (Scheme 8 c).

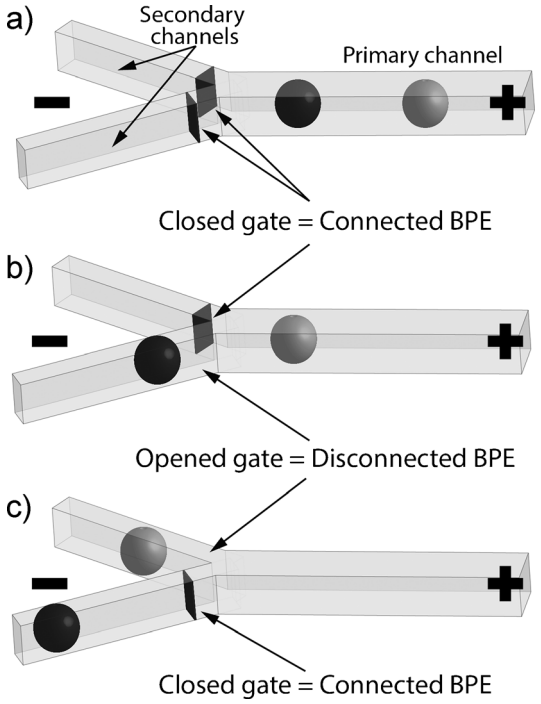

Scheme 8.

5.5. Dual-Channel BPE Focusing

Thus far, we have only discussed BPE focusing studies in which the BPE is embedded within a single channel (Scheme 7 a and 8). Recently, however, we have shown that there are some compelling reasons to consider the dual-channel configuration illustrated in Scheme 9 a.[29,31] The basic operating principles of the dual-channel approach are analogous to those of a single-channel device. Specifically, ΔE_{elec} must

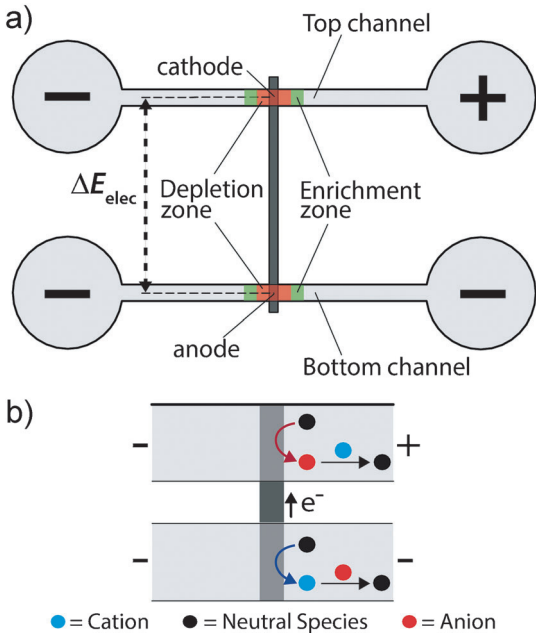

Scheme 9.

exceed the potential required for water oxidation and reduction. If this condition is met, water oxidation [Eq. (2)] will lead to H^+ formation at the anodic pole of the BPE in the bottom channel, while water reduction [Eq. (3)] generates OH^- at the cathodic pole in the top channel. If an appropriately charged buffer capable of being neutralized by the products of water electrolysis is placed in either channel, an ion depletion zone, and thus an electric field gradient, results. For example, in the top channel, $TrisH^+$ may be neutralized by OH^-, or, in the bottom channel, acetate buffer may be neutralized by H^+ (Scheme 9b) to produce an electric field gradient that is suitable for enrichment.

Using the dual-channel device, we have achieved EFs of up to 142000-fold at rates as high as 71-fold/s. These excellent figures of merit are achievable because this configuration decouples E_{tot} and ΔE_{elec}. This means that higher values of E_{tot} may be applied without generating gas bubbles at the BPE. Moreover, higher E_{tot} values increase the rate at which the analyte is transported from the channel reservoirs to the enrichment zone, while simultaneously steepening the local electric field gradient. As discussed in Section 5.3, the latter situation leads to a narrower and more highly enriched analyte band.

A combination of interesting electric field gradients and mass transport conditions can be achieved using the dual-channel configuration, and one of these is illustrated in Figure 12a. This type of gradient results in the simultaneous separation and enrichment of anions and cations in the bottom channel. Here, PDF is directed from left to right, while the direction of EM depends on the charge on the tracer. At the channel center, where there is no electric field strength, ions experience no EM; therefore, their net velocity is dictated exclusively by convection. To the left of the BPE anode, anions move toward the channel center by both EM and PDF. In the same region, cations also experience PDF toward the channel center, but EM is in the opposite direction. When the forces of EM and PDF balance one another, the net velocity of the cations is zero and they enrich. An analogous argument applies to the right side of the BPE anode for anion enrichment. For example, in Figure 12b PDF is directed from left to right in the bottom channel. To the left of the BPE anode (indicated by dashed lines), $[Ru(bpy)_3]^{2+}$ enriches while $BODIPY^{2-}$ enriches to its right. This fluorescence micrograph was collected using a filter set capable of detecting both $BODIPY^{2-}$ and $[Ru(bpy)_3]^{2+}$. Three seconds after Figure 12b was collected, another fluorescence micrograph (Figure 12c) was recorded using a filter set that only detects $BODIPY^{2-}$. In this micrograph, only $BODIPY^{2-}$ enrichment is observed, thereby confirming the identity of the two enriched bands.

Finally, we have very recently shown that a dual-channel BPE configuration can be used to partially desalinate seawater.[125] In this case, Cl^-, present at high concentration in seawater, is oxidized to neutral Cl_2 at the BPE anode. This local reduction in the number of ions results in an electric field gradient that shunts other ions into a nearby third channel. Using this approach, it is possible to remove ca. 25% of the ions from seawater with high energy efficiency. Recent simulations suggest that slight changes to the experimental configuration could lead to a much higher degree of desalination.

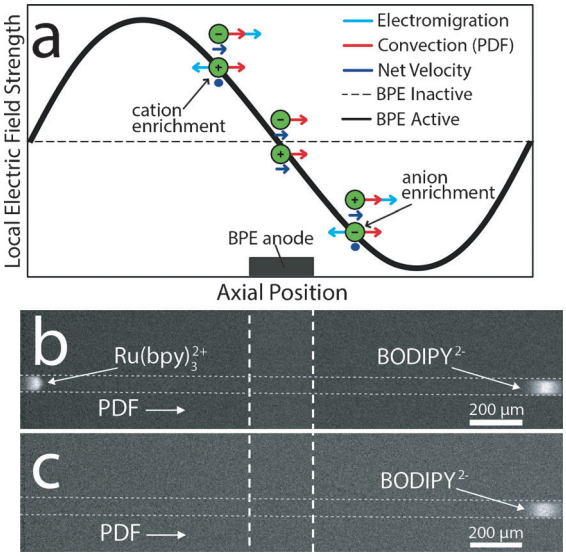

Figure 12. a) Schematic illustration showing the direction of convection, EM, and the net velocity of tracers in the bottom channel of a two-channel microfluidic device. b) Fluorescence micrograph, obtained using a filter set capable of detecting both tracers, showing the location of the enriched bands of $BODIPY^{2-}$ and $[Ru(bpy)_3]^{2+}$ in the bottom channel. The location of the BPE is indicated by dashed white lines and the dotted gray lines show the microchannel walls. $E_{tot} = 30$ V was applied to the positive reservoir (Scheme 9) and the others were at ground. The solution was 40.0 mM acetate buffer. c) Fluorescence micrograph collected 3 s after (b) using a filter set sensitive only to $BODIPY^{2-}$. Adapted with permission from Ref. [31]. Copyright 2012 The Royal Society of Chemistry.

6. Microswimmers

In recent years there have been a number of truly remarkable reports of mobile BPEs, sometimes called microswimmers, that exhibit a function not so different from the miniature submarine in the classic 1966 movie "Fantastic Voyage".[20] Mobility is possible because of one of the key attributes of BPEs mentioned in Section 2: no external connection is required for their operation. Particular functions of mobile BPEs are achieved by changing the composition of the BPE itself, the solution, or the applied electric field. Though the idea of autonomous moving objects and motors has been discussed for many years, recent developments using BPEs have provided a means for implementation.[20]

6.1. Self-Powered, Mobile BPEs

Mallouk, Sen, and co-workers were the first to use self-powered BPEs as nanomotors.[17] The early nanomotors were bimetallic rods having lengths of ca. 1 μm and diameters of ca. 400 nm with different metals, such as Au and Pt,[17] at their ends. Initially, it was believed that the motion of the rods was

due to the evolution of O_2, arising from the catalytic decomposition of H_2O_2 at the Pt end. This was thought to disturb the interfacial tension of the water near the rods, causing them to move in the direction of the Pt end.[17,18,99–102] However, the movement of the nanorods was later attributed to bipolar electrochemistry.[103] The basic idea is that electrons generated from the electrocatalytic oxidation of H_2O_2 at the anodic pole are used for a reduction reaction, such as the ORR, at the cathodic pole. This hypothesis was confirmed by synthesizing a series of nanorods consisting of various metals having different electrocatalytic properties.[103] Moreover, the addition of an insulating layer between the anodic and cathodic poles of the BPE blocked the flow of electrons and rendered the nanorods immobile. Finally, by introducing magnetic segments to the nanorods, the direction of their motion could be controlled, thereby enhancing their technological versatility.[18]

Wang and co-workers have also played an important role in the field of BPE nanomotors.[19] They reported improved efficiencies and achieved speeds of 94 $\mu m\,s^{-1}$ by introducing CNTs to the Pt end and adding hydrazine to the solution.[104] By incorporating other metal pairs and alloys, speeds could be further enhanced.[105,106] Wang and co-workers also reported that mobile BPEs could be used for sensors. For example, they detected Ag^+ in a H_2O_2 solution using Au-Pt nanomotors.[107] This function arises, because Ag^+ is easier to reduce than O_2. The same group later reported similar methods for the capture and isolation of biologically relevant species (e.g. cancer cells, DNA, and RNA),[108–110] oil droplets in water,[111] and other species.[112,113] They used nanomotors to "write" on a surfaces.[114]

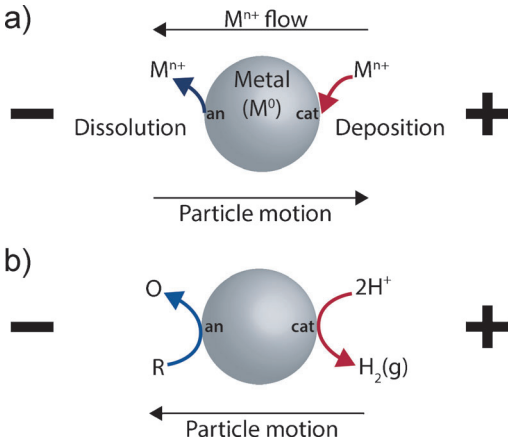

Scheme 10.

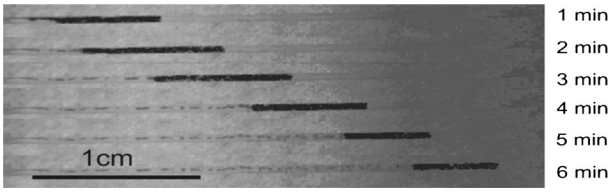

Figure 13. Optical micrographs as a function of time illustrating the concept of self-regeneration. A Zn wire was formed at an electrode by electrodeposition of Zn^{2+} inside a glass capillary. The Zn wire was freed by removing the electrode from the solution. $E_{tot} = 125$ V was applied between driving electrodes at the ends of the capillary. This resulted in oxidation of Zn at the BPE anode and deposition at its cathode. This process results in apparent movement of the Zn wire. Reprinted with permission from Ref. [115]. Copyright 2010 American Chemical Society.

6.2. BPE Swimmers Powered by an External Electric Field

Kuhn and Loget used bipolar electrochemistry for the directed linear motion of metallic objects by a process they called self-regeneration.[115] This approach is based on the simultaneous dissolution of a BPE at its anodic pole and subsequent deposition of the same metal onto the cathodic pole in an externally applied electric field. Conceptually, the principle is similar to that reported earlier by Bradley and co-workers (Scheme 5a and 10a).[60] In the present case, a Zn BPE filament produced in a capillary was electrochemically dissolved at the anodic pole and redeposited at the cathodic pole. This resulted in an effective speed of ca. 60 $\mu m\,s^{-1}$ (Figure 13).

In addition to self-regeneration, other bipolar electrochemical processes can also trigger BPE movement in an electric field. For example, Kuhn and Loget designed a method for linear and rotational movement of BPEs in solution.[21] In this case, the BPE—a metallic bead—moves due to the formation of O_2 and H_2 bubbles arising from water oxidation and hydrogen evolution, respectively, at opposite sides of the sphere (Scheme 10b and Figure 2a). Because the volume of H_2 produced is twice as high as the amount of O_2, the BPE is propelled toward the negative driving electrode. The speed of the BPE could be increased by suppressing O_2 evolution at the anodic pole, which reduces the degree of thrust arising from O_2 bubbles (Figure 2b).[21] This was accomplished by adding hydroquinone, which is more easily oxidized than water, to the solution. Kuhn and co-workers used this same approach to achieve vertical and horizontal rotation of a BPE by modifying its shape,[21] as well as vertical movement of the BPEs in capillaries.[22]

As discussed in Section 3.2, the same group was able to produce Janus-type carbon microtube BPEs modified with Pt at just one pole. These BPEs were later used as microswimmers, which were propelled by H_2O_2 decomposition at the Pt end.[116] Linear and rotational movement of the microswimmers was also possible by controlling the placement of the Pt deposition on the BPE, and their motion could be turned off and on by manipulation of the external electric field.[117]

Sojic, Kuhn, and co-workers also demonstrated that BPE swimmers are capable of generating ECL emission when the oxidation that triggers ECL is coupled to water reduction at the cathodic pole of a carbon bead BPE.[23] Along these same lines, Kuhn, Bouffier, and co-workers showed that BPEs can operate as a wireless electrochemical globe valve, where electrogenerated H_2 bubbles cause the valve to lift and open.[118]

7. Summary and Outlook

The objective of this Review is to stimulate additional interest in bipolar electrochemistry, especially in subdisciplines of science that are able to utilize its particular characteristics. The latter are represented by the examples in the foregoing discussion, but the principal attribute is that BPEs can be activated in the absence of an ohmic contact. The low cost, ease of operation, and simple instrumentation required for bipolar electrochemistry have their origin in this wireless-contact principle.

One consequence of wireless operation, which our group introduced several years ago, is that thousands of electrodes can be controlled simultaneously (Figure 1) with just a battery or a DC power supply. Looking to the future, it seems obvious that BPEs will find more applications to chemical and biological sensing due to the extreme simplicity of the method. For example, we are presently investigating the integration of BPEs into low-cost paper microfluidic devices[119] for point-of-care applications and other situations in which complicated instrumentation is not desirable.[120,121]

The quick and simple screening capabilities of BPEs, which were discussed in Section 4.6 in the context of electrocatalysis, will also be adapted to other types of screening and selection processes in the future. For example, applications to DNA, protein, and glycan arrays are certainly worth investigating. A specific case in which BPEs could possibly provide benefit is enabling the type of site-selective electrochemical reaction screening method used by Moeller and co-workers.[122]

The principle of wireless contact also makes it possible to carry out electrochemical experiments on mobile electrodes. The potential of these microswimmers are embodied in the work of Mallouk, Sen, Kuhn, and Wang discussed earlier, but we believe that many more interesting applications will evolve in future years in the fields of medicine, electronics, and chemical sensing. For example, one could imagine self-assembling electronic circuits using this approach, or perhaps search a solution for a small number of target molecules.

As discussed in the Review, Kuhn and others have pioneered applications of BPEs to materials science and materials chemistry, and it is very likely that even more significant types of structures and synthetic approaches, which are difficult or impossible to prepare by other means, are just around the corner.

Another surprising fact is that bipolar electrochemistry plays a key role in certain widespread applications, even though the bipolar contribution has only recently been discovered. For example, Amatore and co-workers have shown that bipolar electrochemistry is associated with feedback behavior in scanning electrochemical microscopy (SECM).[123] Of even more significance, Zhang and his colleagues demonstrated that the behavior of the types of carbon fiber electrodes used to study biological cells are often dominated by bipolar electrochemical principles.[58] No doubt there are other examples like these in which the hidden hand of BPEs will eventually be revealed.

Glossary and Symbols

BPE	bipolar electrode
CNT	carbon nanotube
CE	capillary electrophoresis
$E°$	standard potential
ΔE_{elec}	potential difference between the bipolar electrode poles
E_{elec}	potential of the floating bipolar electrode
E_{tot}	externally applied potential bias between driving electrodes
ECL	electrogenerated chemiluminescence
EOF	electroosmotic flow
EM	electromigration
EF	enrichment factor
l_{elec}	length of the bipolar electrode
$l_{channel}$	length of the channel or between driving electrodes
η_{an}	anodic overpotential
η_{cat}	cathodic overpotential
i_{tot}	total current
i_{an}	anodic current
i_{cat}	cathodic current
R_S	solution resistance
R_{elec}	sum of electrode resistances
NP	nanoparticle
ORR	oxygen reduction reaction
PDMS	poly(dimethylsiloxane)
u_{ep}	electrophoretic velocity
μ_{ep}	electrophoretic mobility
V_l	local electric field strength
PDF	pressure-driven flow

Acknowledgement

We gratefully acknowledge financial support from the Chemical Sciences, Geosciences, and Biosciences Division, Office of Basic Energy Sciences, Office of Science, U.S. Department of Energy (Contract No. DE-FG02-06ER15758) for support of our work involving bipolar electrode focusing. We also acknowledge support from the U.S. Army Research Office (grant no. W911NF-07-1-0330) and the U.S. Defense Threat Reduction Agency for support of our studies of bipolar electrodes for chemical sensing. The Robert A. Welch Foundation (Grant F-0032) provides sustained support for our research. We also acknowledge major contributions to our studies of BPEs by our long-time collaborators Prof. Ulrich Tallarek and Dr. Dzmitry Hlushkou (Philipps-Universität Marburg). We are particularly indebted to our former research group members Prof. Julio Alvarez (Virginia Commonwealth University) and Prof. Wei Zhan (Auburn University) whose pioneering experiments with BPEs more than a decade ago led to a renaissance in this subfield of electrochemistry. Numerous other group members, past and present, have also made important contributions to our work, and we recognize their contributions through the science reported herein.

Received: February 2, 2013
Published online: July 10, 2013

[1] J. R. Backhurst, J. M. Coulson, F. Goodridge, R. E. Plimley, M. Fleischmann, *J. Electrochem. Soc.* **1969**, *116*, 1600 – 1607.
[2] M. Fleischmann, J. W. Oldfield, *J. Electroanal. Chem. Interfacial Electrochem.* **1971**, *29*, 211 – 30.
[3] F. Goodridge, C. J. H. King, A. R. Wright, *Electrochim. Acta* **1977**, *22*, 347 – 352.
[4] F. Goodridge, C. J. H. King, A. R. Wright, *Electrochim. Acta* **1977**, *22*, 1087 – 1091.
[5] R. E. Plimley, A. R. Wright, *Chem. Eng. Sci.* **1984**, *39*, 395 – 405.
[6] M. Fleischmann, J. Ghoroghchian, D. Rolison, S. Pons, *J. Phys. Chem.* **1986**, *90*, 6392 – 6400.
[7] K. G. Ellis, R. E. W. Jansson, *J. Appl. Electrochem.* **1981**, *11*, 531 – 535.
[8] A. Manji, C. W. Oloman, *J. Appl. Electrochem.* **1987**, *17*, 532 – 544.
[9] J. K. Lee, L. W. Shemilt, H. S. Chun, *J. Appl. Electrochem.* **1989**, *19*, 877 – 881.
[10] E. Smotkin, A. J. Bard, A. Campion, M. A. Fox, T. Mallouk, S. E. Webber, J. M. White, *J. Phys. Chem.* **1986**, *90*, 4604 – 4607.
[11] S. Cervera-March, E. S. Smotkin, A. J. Bard, A. Campion, M. A. Fox, T. Mallouk, S. E. Webber, J. M. White, *J. Electrochem. Soc.* **1988**, *135*, 567 – 573.
[12] K. Wiesener, D. Ohms, G. Benczúr-Ürmössy, M. Berthold, F. Haschka, *J. Power Sources* **1999**, *84*, 248 – 258.
[13] B. C. H. Steele, A. Heinzel, *Nature* **2001**, *414*, 345 – 352.
[14] A. Hermann, T. Chaudhuri, P. Spagnol, *Int. J. Hydrogen Energy* **2005**, *30*, 1297 – 1302.
[15] C. Amatore, A. R. Brown, L. Thouin, J.-S. Warkocz, *C. R. Acad. Sci. Ser. IIc* **1998**, *1*, 509 – 515.
[16] K.-F. Chow, F. Mavré, J. A. Crooks, B.-Y. Chang, R. M. Crooks, *J. Am. Chem. Soc.* **2009**, *131*, 8364 – 8365.
[17] W. F. Paxton, K. C. Kistler, C. C. Olmeda, A. Sen, S. K. St. Angelo, Y. Cao, T. E. Mallouk, P. E. Lammert, V. H. Crespi, *J. Am. Chem. Soc.* **2004**, *126*, 13424 – 13431.
[18] T. R. Kline, W. F. Paxton, T. E. Mallouk, A. Sen, *Angew. Chem.* **2005**, *117*, 754 – 756; *Angew. Chem. Int. Ed.* **2005**, *44*, 744 – 746.
[19] J. Wang, K. M. Manesh, *Small* **2010**, *6*, 338 – 345.
[20] S. Sengupta, M. E. Ibele, A. Sen, *Angew. Chem.* **2012**, *124*, 8560 – 8571; *Angew. Chem. Int. Ed.* **2012**, *51*, 8434 – 8445.
[21] G. Loget, A. Kuhn, *Nat. Commun.* **2011**, *2*, 535.
[22] G. Loget, A. Kuhn, *Lab Chip* **2012**, *12*, 1967 – 71.
[23] M. Sentic, G. Loget, D. Manojlovic, A. Kuhn, N. Sojic, *Angew. Chem.* **2012**, *124*, 11446 – 11450; *Angew. Chem. Int. Ed.* **2012**, *51*, 11284 – 11288.
[24] S. Inagi, Y. Ishiguro, M. Atobe, T. Fuchigami, *Angew. Chem.* **2010**, *122*, 10334 – 10337; *Angew. Chem. Int. Ed.* **2010**, *49*, 10136 – 10139.
[25] Y. Ishiguro, S. Inagi, T. Fuchigami, *Langmuir* **2011**, *27*, 7158 – 7162.
[26] D. R. Laws, D. Hlushkou, R. K. Perdue, U. Tallarek, R. M. Crooks, *Anal. Chem.* **2009**, *81*, 8923 – 8929.
[27] R. K. Perdue, D. R. Laws, D. Hlushkou, U. Tallarek, R. M. Crooks, *Anal. Chem.* **2009**, *81*, 10149 – 10155.
[28] R. K. Anand, E. Sheridan, D. Hlushkou, U. Tallarek, R. M. Crooks, *Lab Chip* **2011**, *11*, 518 – 527.
[29] R. K. Anand, E. Sheridan, K. N. Knust, R. M. Crooks, *Anal. Chem.* **2011**, *83*, 2351 – 2358.
[30] E. Sheridan, K. N. Knust, R. M. Crooks, *Analyst* **2011**, *136*, 4134 – 4137.
[31] K. N. Knust, E. Sheridan, R. K. Anand, R. M. Crooks, *Lab Chip* **2012**, *12*, 4107 – 4114.
[32] K. Scida, E. Sheridan, R. M. Crooks, *Lab Chip* **2013**, *13*, 2292 – 2299.
[33] E. Sheridan, D. Hlushkou, K. N. Knust, U. Tallarek, R. M. Crooks, *Anal. Chem.* **2012**, *84*, 7393 – 7399.
[34] W. Zhan, J. Alvarez, R. M. Crooks, *J. Am. Chem. Soc.* **2002**, *124*, 13265 – 13270.
[35] K.-F. Chow, F. Mavré, R. M. Crooks, *J. Am. Chem. Soc.* **2008**, *130*, 7544 – 7545.
[36] F. Mavré, K.-F. Chow, E. Sheridan, B.-Y. Chang, J. A. Crooks, R. M. Crooks, *Anal. Chem.* **2009**, *81*, 6218 – 6225.
[37] B.-Y. Chang, J. A. Crooks, K.-F. Chow, F. Mavré, R. M. Crooks, *J. Am. Chem. Soc.* **2010**, *132*, 15404 – 15409.
[38] K.-F. Chow, B.-Y. Chang, B. A. Zaccheo, F. Mavré, R. M. Crooks, *J. Am. Chem. Soc.* **2010**, *132*, 9228 – 9229.
[39] B.-Y. Chang, F. Mavré, K.-F. Chow, J. A. Crooks, R. M. Crooks, *Anal. Chem.* **2010**, *82*, 5317 – 5322.
[40] S. E. Fosdick, J. A. Crooks, B.-Y. Chang, R. M. Crooks, *J. Am. Chem. Soc.* **2010**, *132*, 9226 – 9227.
[41] I. Dumitrescu, R. K. Anand, S. E. Fosdick, R. M. Crooks, *J. Am. Chem. Soc.* **2011**, *133*, 4687 – 4689.
[42] S. E. Fosdick, R. M. Crooks, *J. Am. Chem. Soc.* **2012**, *134*, 863 – 866.
[43] B.-Y. Chang, K.-F. Chow, J. A. Crooks, F. Mavré, R. M. Crooks, *Analyst* **2012**, *137*, 2827 – 2833.
[44] S. E. Fosdick, S. P. Berglund, C. B. Mullins, R. M. Crooks, *Anal. Chem.* **2013**, *85*, 2493 – 2499.
[45] A. Arora, J. C. T. Eijkel, W. E. Morf, A. Manz, *Anal. Chem.* **2001**, *73*, 3282 – 3288.
[46] R. H. Terrill, K. M. Balss, Y. M. Zhang, P. W. Bohn, *J. Am. Chem. Soc.* **2000**, *122*, 988 – 989.
[47] J. Duval, J. M. Kleijn, H. P. van Leeuwen, *J. Electroanal. Chem.* **2001**, *505*, 1 – 11.
[48] F. Mavré, R. K. Anand, D. R. Laws, K.-F. Chow, B.-Y. Chang, J. A. Crooks, R. M. Crooks, *Anal. Chem.* **2010**, *82*, 8766 – 8774.
[49] J. F. L. Duval, G. K. Huijs, W. F. Threels, J. Lyklema, H. P. van Leeuwen, *J. Colloid Interface Sci.* **2003**, *260*, 95 – 106.
[50] J. F. L. Duval, M. Minor, J. Cecilia, H. P. van Leeuwen, *J. Phys. Chem. B* **2003**, *107*, 4143 – 4155.
[51] J. F. L. Duval, H. P. van Leeuwen, J. Cecilia, J. Galceran, *J. Phys. Chem. B* **2003**, *107*, 6782 – 6800.
[52] J. F. L. Duval, *J. Colloid Interface Sci.* **2004**, *269*, 211 – 223.
[53] J. F. L. Duval, J. Buffle, H. P. van Leeuwen, *J. Phys. Chem. B* **2006**, *110*, 6081 – 6094.
[54] A. J. Bard, L. R. Faulkner, *Electrochemical Methods: Fundamentals and Applications*, *2nd ed.*, Wiley, New York, **2001**.
[55] P. G. Ndungu, *The Use of Bipolar Electrochemistry in Nanoscience*: *Contact Free Methods for the Site Selective Modification of Nanostructured Carbon Materials*, Drexel University, Philadelphia, **2004**.
[56] D. Plana, G. Shul, M. J. Stephenson, R. A. W. Dryfe, *Electrochem. Commun.* **2009**, *11*, 61 – 64.
[57] D. Plana, F. G. E. Jones, R. A. W. Dryfe, *J. Electroanal. Chem.* **2010**, *646*, 107 – 113.
[58] J. P. Guerrette, S. M. Oja, B. Zhang, *Anal. Chem.* **2012**, *84*, 1609 – 1616.
[59] J. T. Cox, J. P. Guerrette, B. Zhang, *Anal. Chem.* **2012**, *84*, 8797 – 804.
[60] J.-C. Bradley, H. M. Chen, J. Crawford, J. Eckert, K. Ernazarova, T. Kurzeja, M. D. Lin, M. McGee, W. Nadler, S. G. Stephens, *Nature* **1997**, *389*, 268 – 271.
[61] J.-C. Bradley, J. Crawford, K. Ernazarova, M. McGee, S. G. Stephens, *Adv. Mater.* **1997**, *9*, 1168 – 1171.
[62] J.-C. Bradley, J. Crawford, M. McGee, S. G. Stephens, *J. Electrochem. Soc.* **1998**, *145*, L45 – L47.
[63] J.-C. Bradley, S. Dengra, G. A. Gonzalez, G. Marshall, F. V. Molina, *J. Electroanal. Chem.* **1999**, *478*, 128 – 139.
[64] J.-C. Bradley, Z. M. Ma, E. Clark, J. Crawford, S. G. Stephens, *J. Electrochem. Soc.* **1999**, *146*, 194 – 198.
[65] J.-C. Bradley, S. Babu, B. Carroll, A. Mittal, *J. Electroanal. Chem.* **2002**, *522*, 75 – 85.

[66] J.-C. Bradley, Z. Ma, S. G. Stephens, *Adv. Mater.* **1999**, *11*, 374 – 378.
[67] J.-C. Bradley, Z. M. Ma, *Angew. Chem.* **1999**, *111*, 1768 – 1771; *Angew. Chem. Int. Ed.* **1999**, *38*, 1663 – 1666.
[68] J.-C. Bradley, S. Babu, P. Ndungu, *Fullerenes Nanotubes Carbon Nanostruct.* **2005**, *13*, 227 – 237.
[69] C. Warakulwit, T. Nguyen, J. Majimel, M.-H. Delville, V. Lapeyre, P. Garrigue, V. Ravaine, J. Limtrakul, A. Kuhn, *Nano Lett.* **2008**, *8*, 500 – 504.
[70] G. Loget, G. Larcade, V. Lapeyre, P. Garrigue, C. Warakulwit, J. Limtrakul, M. H. Delville, V. Ravaine, A. Kuhn, *Electrochim. Acta* **2010**, *55*, 8116 – 8120.
[71] G. Loget, V. Lapeyre, P. Garrigue, C. Warakulwit, J. Limtrakul, M. H. Delville, A. Kuhn, *Chem. Mater.* **2011**, *23*, 2595 – 2599.
[72] G. Loget, J. Roche, A. Kuhn, *Adv. Mater.* **2012**, *24*, 5111 – 5116.
[73] Z. Fattah, P. Garrigue, V. Lapeyre, A. Kuhn, L. Bouffier, *J. Phys. Chem. C* **2012**, *116*, 22021 – 22027.
[74] G. Loget, J. Roche, E. Gianessi, L. Bouffier, A. Kuhn, *J. Am. Chem. Soc.* **2012**, *134*, 20033 – 20036.
[75] Z. Fattah, J. Roche, P. Garrigue, D. Zigah, L. Bouffier, A. Kuhn, *ChemPhysChem* **2013**, DOI: 10.1002/cphc.201300068.
[76] D. Xu, K. Shou, B. J. Nelson, *Microelectron. Eng.* **2011**, *88*, 2703 – 2706.
[77] C. Ulrich, O. Andersson, L. Nyholm, F. Björefors, *Angew. Chem.* **2008**, *120*, 3076 – 3078; *Angew. Chem. Int. Ed.* **2008**, *47*, 3034 – 3036.
[78] S. Ramakrishnan, C. Shannon, *Langmuir* **2010**, *26*, 4602 – 4606.
[79] R. Ramaswamy, C. Shannon, *Langmuir* **2011**, *27*, 878 – 881.
[80] S. Inagi, Y. Ishiguro, N. Shida, T. Fuchigami, *J. Electrochem. Soc.* **2012**, *159*, G146 – G150.
[81] Y. Ishiguro, S. Inagi, T. Fuchigami, *J. Am. Chem. Soc.* **2012**, *134*, 4034 – 6.
[82] N. Shida, Y. Ishiguro, M. Atobe, T. Fuchigami, S. Inagi, *ACS Macro Lett.* **2012**, *1*, 656 – 659.
[83] O. Klett, L. Nyholm, *Anal. Chem.* **2003**, *75*, 1245 – 1250.
[84] J. Wang, *Talanta* **2002**, *56*, 223 – 231.
[85] O. Ordeig, N. Godino, J. del Campo, F. X. Muñoz, F. Nikolajeff, L. Nyholm, *Anal. Chem.* **2008**, *80*, 3622 – 3632.
[86] A. J. Bard, *Electrogenerated Chemiluminescence*, Marcel Dekker, New York, **2004**.
[87] M.-S. Wu, G.-s. Qian, J.-J. Xu, H.-Y. Chen, *Anal. Chem.* **2012**, *84*, 5407 – 5414.
[88] M.-S. Wu, D.-J. Yuan, J.-J. Xu, H.-Y. Chen, *Chem. Sci.* **2013**, *4*, 1182 – 1188.
[89] W. Zhan, R. M. Crooks, *J. Am. Chem. Soc.* **2003**, *125*, 9934 – 9935.
[90] P. Juskova, P. Neuzil, A. Manz, F. Foret, *Lab Chip* **2013**, *13*, 781 – 784.
[91] X. Lin, L. Zheng, G. Gao, Y. Chi, G. Chen, *Anal. Chem.* **2012**, *84*, 7700 – 7707.
[92] J. P. Guerrette, S. J. Percival, B. Zhang, *J. Am. Chem. Soc.* **2013**, *135*, 855 – 61.
[93] R. Dhopeshwarkar, D. Hlushkou, M. Nguyen, U. Tallarek, R. M. Crooks, *J. Am. Chem. Soc.* **2008**, *130*, 10480 – 10481.
[94] J. G. Shackman, D. Ross, *Electrophoresis* **2007**, *28*, 556 – 571.
[95] S. E. Yalcin, A. Sharma, S. Qian, S. W. Joo, O. Baysal, *Electrophoresis* **2010**, *31*, 3711 – 3718.
[96] S. E. Yalcin, A. Sharma, S. Qian, S. W. Joo, O. Baysal, *Sens. Actuators B* **2011**, *153*, 277 – 283.
[97] D. Hlushkou, R. K. Perdue, R. Dhopeshwarkar, R. M. Crooks, U. Tallarek, *Lab Chip* **2009**, *9*, 1903 – 1913.
[98] E. Sheridan, D. Hlushkou, R. K. Anand, D. R. Laws, U. Tallarek, R. M. Crooks, *Anal. Chem.* **2011**, *83*, 6746 – 6753.
[99] T. R. Kline, W. F. Paxton, Y. Wang, D. Velegol, T. E. Mallouk, A. Sen, *J. Am. Chem. Soc.* **2005**, *127*, 17150 – 17151.
[100] W. F. Paxton, A. Sen, T. E. Mallouk, *Chemistry* **2005**, *11*, 6462 – 6470.
[101] W. F. Paxton, P. T. Baker, T. R. Kline, Y. Wang, T. E. Mallouk, A. Sen, *J. Am. Chem. Soc.* **2006**, *128*, 14881 – 14888.
[102] W. F. Paxton, S. Sundararajan, T. E. Mallouk, A. Sen, *Angew. Chem.* **2006**, *118*, 5546 – 5556; *Angew. Chem. Int. Ed.* **2006**, *45*, 5420 – 5429.
[103] Y. Wang, R. M. Hernandez, D. J. Bartlett, J. M. Bingham, T. R. Kline, A. Sen, T. E. Mallouk, *Langmuir* **2006**, *22*, 10451 – 10456.
[104] R. Laocharoensuk, J. Burdick, J. Wang, *ACS Nano* **2008**, *2*, 1069 – 1075.
[105] S. Sattayasamitsathit, W. Gao, P. Calvo-Marzal, K. M. Manesh, J. Wang, *ChemPhysChem* **2010**, *11*, 2802 – 2805.
[106] U. K. Demirok, R. Laocharoensuk, K. M. Manesh, J. Wang, *Angew. Chem.* **2008**, *120*, 9489 – 9491; *Angew. Chem. Int. Ed.* **2008**, *47*, 9349 – 9351.
[107] D. Kagan, P. Calvo-Marzal, S. Balasubramanian, S. Sattayasamitsathit, K. M. Manesh, G. U. Flechsig, J. Wang, *J. Am. Chem. Soc.* **2009**, *131*, 12082 – 12083.
[108] J. Wu, S. Balasubramanian, D. Kagan, K. M. Manesh, S. Campuzano, J. Wang, *Nat. Commun.* **2010**, *1*, 36.
[109] S. Balasubramanian, D. Kagan, C. M. J. Hu, S. Campuzano, M. J. Lobo-Castanon, N. Lim, D. Y. Kang, M. Zimmerman, L. F. Zhang, J. Wang, *Angew. Chem.* **2011**, *123*, 4247 – 4250; *Angew. Chem. Int. Ed.* **2011**, *50*, 4161 – 4164.
[110] D. Kagan, S. Campuzano, S. Balasubramanian, F. Kuralay, G. U. Flechsig, J. Wang, *Nano Lett.* **2011**, *11*, 2083 – 2087.
[111] M. Guix, J. Orozco, M. García, W. Gao, S. Sattayasamitsathit, A. Merkoçi, A. Escarpa, J. Wang, *ACS Nano* **2012**, *6*, 4445 – 4451.
[112] J. Wang, *ACS Nano* **2009**, *3*, 4 – 9.
[113] S. Campuzano, D. Kagan, J. Orozco, J. Wang, *Analyst* **2011**, *136*, 4621 – 4630.
[114] K. M. Manesh, S. Balasubramanian, J. Wang, *Chem. Commun.* **2010**, *46*, 5704 – 5706.
[115] G. Loget, A. Kuhn, *J. Am. Chem. Soc.* **2010**, *132*, 15918 – 15919.
[116] Z. Fattah, G. Loget, V. Lapeyre, P. Garrigue, C. Warakulwit, J. Limtrakul, L. Bouffier, A. Kuhn, *Electrochim. Acta* **2011**, *56*, 10562 – 10566.
[117] P. Calvo-Marzal, K. M. Manesh, D. Kagan, S. Balasubramanian, M. Cardona, G. U. Flechsig, J. Posner, J. Wang, *Chem. Commun.* **2009**, 4509 – 4511.
[118] L. Bouffier, A. Kuhn, *Nanoscale* **2013**, *5*, 1305 – 1309.
[119] A. W. Martinez, S. T. Phillips, G. M. Whitesides, E. Carrilho, *Anal. Chem.* **2010**, *82*, 3 – 10.
[120] H. Liu, R. M. Crooks, *J. Am. Chem. Soc.* **2011**, *133*, 17564 – 17566.
[121] H. Liu, Y. Xiang, Y. Lu, R. M. Crooks, *Angew. Chem.* **2012**, *124*, 7031 – 7034; *Angew. Chem. Int. Ed.* **2012**, *51*, 6925 – 6928.
[122] J. Tian, K. Maurer, E. Tesfu, K. D. Moeller, *J. Am. Chem. Soc.* **2005**, *127*, 1392 – 1393.
[123] A. I. Oleinick, D. Battistel, S. Daniele, I. Svir, C. Amatore, *Anal. Chem.* **2011**, *83*, 4887 – 4893.
[124] G. Loget, D. Zigah, L. Bouffier, N. Sojic, A. Kuhn, *Acc. Chem. Res.* **2013**, DOI: 10.1021/ar400039k.
[125] K. N. Knust, D. Hlushkou, R. K. Anand, U. Tallarek, R. M. Crooks, *Angew. Chem.* **2013**, *125*, DOI: 10.1002/ange.201302577; *Angew. Chem. Int. Ed.* **2013**, *52*, DOI: 10.1002/anie.201302577.